Polar cap boundary layer waves: An auroral zone phenomenon

Bruce T. Tsurutani, John K. Arballo, Carlos Galvan, Liwei Dennis Zhang, and Xiao-Yan Zhou

Jet Propulsion Laboratory, California Institute of Technology, Pasadena, California

Gurbax S. Lakhina

Indian Institute of Geomagnetism, Mumbai/Bombay, India

Tohru Hada

Earth System Science and Technology, Kyushu University, Fukuoka, Japan

Jolene S. Pickett and Donald A. Gurnett

Department of Physics and Astronomy, University of Iowa, Iowa City, Iowa

Abstract. Polar cap boundary layer waves are ELF/VLF electric and magnetic waves detected on field lines just adjacent to the polar cap. Intense waves are present at this location essentially all (96%) of the time. The wave latitude-local time distribution is shown to be the same as that of the Feldstein auroral oval, a distribution centered at ~75° at local noon and ~65° at local midnight. The most intense waves are detected coincident with the strongest magnetic field gradients (field-aligned currents). Statistically, the wave intensities are greatest near local noon (10^{-13} mV^2 m^{-1} at 3 kHz) and midnight and are least near dawn and dusk (~5×10^{-15} mV^2 m^{-1} at 3 kHz). The noon and midnight wave intensities increase slightly when the interplanetary magnetic field is directed southward. The dawn and dusk waves appear to be controlled by the solar wind speed. Using high-resolution data, specific frequency bands of electromagnetic whistler-mode waves are identified: ~200 Hz and 1-2 and ~5 kHz. These may correspond to previously identified "magnetic noise bursts" and "auroral hiss", respectively. Assuming cyclotron resonant interactions, the 1- to 5-kHz auroral hiss is shown to be resonant with ~50-eV to ~1.0-keV electrons. Several mechanisms, both resonant (nonlocal) and nonresonant (local), are suggested for the generation of the ~200-Hz electromagnetic waves. Three types of intense electric signals are present: solitary bipolar pulses (electron holes), waves at ~4×10^2 to 6×10^3 Hz (lower hybrid waves), and narrowband waves at ~10 kHz (electrostatic waves near the upper hybrid resonance frequency). Solitary bipolar pulse onset events have been detected for the first time. The bipolar pulses reached 2 mV m^{-1} peak-to-peak amplitudes within 3 ms. An exponential growth rate of 0.72 ms, or 0.25 f_{ce}, was determined. The previously reported "broadband nature" of the polar cap boundary layer (and low-latitude boundary layer) waves is now postulated to be caused by a fast switching between the various electromagnetic and electrostatic modes described above. The polar cap boundary layer waves are most likely a consequence of instabilities associated with auroral zone field-aligned currents carried by 50-eV to 1.0-keV electrons and protons. The currents in turn have been ascribed to be driven by the solar wind-magnetosphere global interaction. One consequence of the presence of the waves at high altitudes is diffusion of magnetosheath plasma into the magnetosphere and magnetospheric plasma out into the magnetosheath (cross-field diffusion, due to parasitic wave-particle interactions). It is speculated that field-aligned currents and similar wave modes will be detected at all planetary magnetospheres.

1. Introduction

Low-latitude (magnetopause) boundary layer (LLBL) ELF-VLF plasma waves have been studied by a variety of spacecraft

missions both at Earth [*Gurnett et al.*, 1979; *Tsurutani et al.*, 1981, 1989; *Gendrin*, 1983; *La Belle and Treumann*, 1988; *Rezeau et al.*, 1986; *Zhu et al.*, 1996; *Song et al.*, 1998] and at Jupiter [*Tsurutani et al.*, 1993, 1997]. The waves as detected by spectral analyses were noted to be "broadband" in electric (E) and magnetic (B) signatures. Because the B/E amplitude ratio did not fit that for a pure whistler mode, it was suggested that the waves were a superposition of electromagnetic whistler mode

waves plus electrostatic signals [*Gurnett et al.*, 1979; *Tsurutani et al.*, 1989, 1997]. Recent analyses of Polar plasma wave data [*Tsurutani* et al., 1998a] have indicated that broadband waves with similar properties exist at lower altitudes on field lines bounding the polar cap (thus they are called polar cap boundary layer (PCBL) waves). It is speculated that these waves are on LLBL magnetic field lines but at lower altitudes. Polar high time resolution data have resolved the cause of the "broadbandedness" of the PCBL waves [*Franz et al.*, 1998; *Tsurutani et al.*, 1998b]. There are indeed whistler-mode emissions present, but the waves are patchy packets only ~10 ms in duration. The packets occur with a variety of frequencies, and integrated over time, a rough power law power spectrum is formed. Superposed with the whistler-mode emissions are electric solitary waves with approximately millisecond durations [*Franz et al.*, 1998; *Tsurutani et al.*, 1998b] (see *Lakhina and Tsurutani* [1999] for a review). Such solitary structures have been observed earlier by the S3-3 [*Temerin et al.*, 1982] and the Viking [*Boström et al.*, 1988; *Koskinen et al.*, 1990] spacecraft. *Pottelette et al.* [1990] detected intense, tens of mV m^{-1} amplitude, broadband, electrostatic bursts lasting 100–200 ms. They noted that the noise bursts were correlated with < 1-keV electron beams and that perpendicular acceleration of plasma ions occurs in connection with the bursts. *Dubouloz et al.* [1991a, 1991b] have modeled the Viking solitary structures in terms of electron acoustic solitons to explain the high-frequency part of the broadband electric noise. Large-amplitude solitary parallel electric field structures have been observed by FAST [*Ergun et al.*, 1998a,1998b; *McFadden et al.*, 1999]. The bipolar electric structures observed by Polar and FAST have positive potentials and are speculated to be electron holes [*Mozer et al.*, 1997; *Franz et al.*, 1998; *Tsurutani et al.*, 1998b; *Ergun et al.*, 1998a, 1998b, 1999; *Goldman et al.*, 1999a, 1999b; *Muschietti et al.*, 1999a, 1999b]. *Bounds et al.* [1999] have found that positive potential solitary structures (electron holes) are associated with electron beams, whereas ion solitary structures are associated with ion beams.

It is the purpose of this paper to report the results of several statistical studies and high time resolution data analyses of the Polar PCBL waves. First, we use 1 year of Polar plasma wave data to determine the latitudinal location of the PCBL waves over a full 24 hours of local time. It will be shown that the latitudinal distribution forms continuous rings about the magnetic poles that are very similar to that of the auroral oval. Second, using the Wind interplanetary magnetic field and plasma data, we study possible interplanetary control or controls of the intensities of the waves. Finally, we will examine and comment on the nature of the waves at different local times. The latter will be done using high time resolution waveform data. In summary, we will comment on the possible role that the PCBL/LLBL/auroral zone plasma waves are playing in the overall magnetospheric physics.

2. Instrument Description

A full description of the plasma wave instrument onboard the Polar spacecraft is given by *Gurnett et al.* [1995]. We will briefly describe here parts of the instrument whose output data are used in this paper.

The plasma wave instrument measures plasma waves in the frequency range from 0.1 Hz to 800 kHz. The instrument consists of a triaxial set of electric dipole antennas, a triaxial set of magnetic search coil antennas, a magnetic loop antenna, and 5 receiver systems. In this study we will use signals from

the antennas processed by a sweep frequency receiver (SFR), by a multichannel analyzer (MCA), and by a high-frequency waveform receiver (HFWR) (there are many other instrument systems that are not used in this study). The SFR provides good frequency resolution with poor time resolution. It provides amplitude measurements in five frequency bands from 26 Hz to 808 kHz. In this study the SFR data are used to identify intervals where PCBL waves are present. The MCA data are used to obtain wave intensities for the PCBL wave intervals. The electric MCA data span a frequency range of 5.6 Hz to 311 kHz in 20 log-spaced channels. The magnetic MCA data span a frequency range of 5.6 Hz to 10 kHz in 14 log-spaced channels. The center frequencies of the MCA channels are indicated in the text ("3 kHz waves" indicates signals from the MCA spectrum channel centered at 3 kHz). In the body of the paper we also refer to electric (E) and magnetic (B) signals. This notation is used to imply spectrum channel outputs without identifying a particular wave mode (both electrostatic and electromagnetic waves have an electric component). Identification of specific wave modes is performed by using simultaneous E and B waveform data. The HFWR data are used to study waves in the time domain. The time resolution is 14 μs. Simultaneous triaxial E and B data during short, selected intervals are available. Rotation of these wave components into magnetic-field-aligned components (the dc magnetic-field is courtesy of C.T. Russell) is performed for intervals of interest. In this coordinate system, the z-axis lies along the local ambient magnetic field direction, $\mathbf{B}_0$. $\hat{x} = (\mathbf{r} \times \hat{z})/|\mathbf{r} \times \hat{z}|$, where $\mathbf{r}$ is the vector from Earth to the spacecraft. The y-axis completes the right-hand system. Because of the very high time resolution nature of this data set, in practice, only limited amounts of data can be analyzed. The "general" wave properties at local noon, dawn, dusk, and midnight discussed in this paper will be determined by a single near-apogee pass which occurred at that local time. It should be noted that a full discussion of the local time dependence of the waves under a variety of solar wind conditions is well beyond the scope of the present work.

For the apogee passes, the wave intervals were divided into 10-min increments. The Polar MCA average, peak, and minimum intensities were calculated and stored. There are 14 frequency channels of B and 20 frequency channels of E; thus a total of 34 × 3 values are stored for each 10-min interval (the MCA data have a 1.3-s time resolution). For the perigee passes, the intervals were divided into 5-min increments and similar calculations were made. The latter time interval was chosen because the perigee PCBL wave durations were much shorter in time (due to the higher spacecraft speeds at perigee).

To study the interplanetary control of the waves, we use the Wind spacecraft solar wind data. Parameters considered are IMF B_z and B_y, the solar wind ram pressure (mNV_{sw}^2), magnetic plus plasma pressure, and $V_{\mathrm{sw}}B_z$. Ten-minute averages of the above quantities were calculated for the apogee intervals, and 5-min averages were calculated for perigee. Using the measured, in situ solar wind velocity and the upstream location of the Wind spacecraft, the convection times of the solar wind plasma and magnetic fields from Wind to the magnetopause nose (assumed to be 10 R_E) were calculated. The solar wind "data parcels" were then time-tagged by the calculated arrival time at the magnetopause. When two or more data parcels occupied the same time intervals (this happens when there were large variations in the solar wind
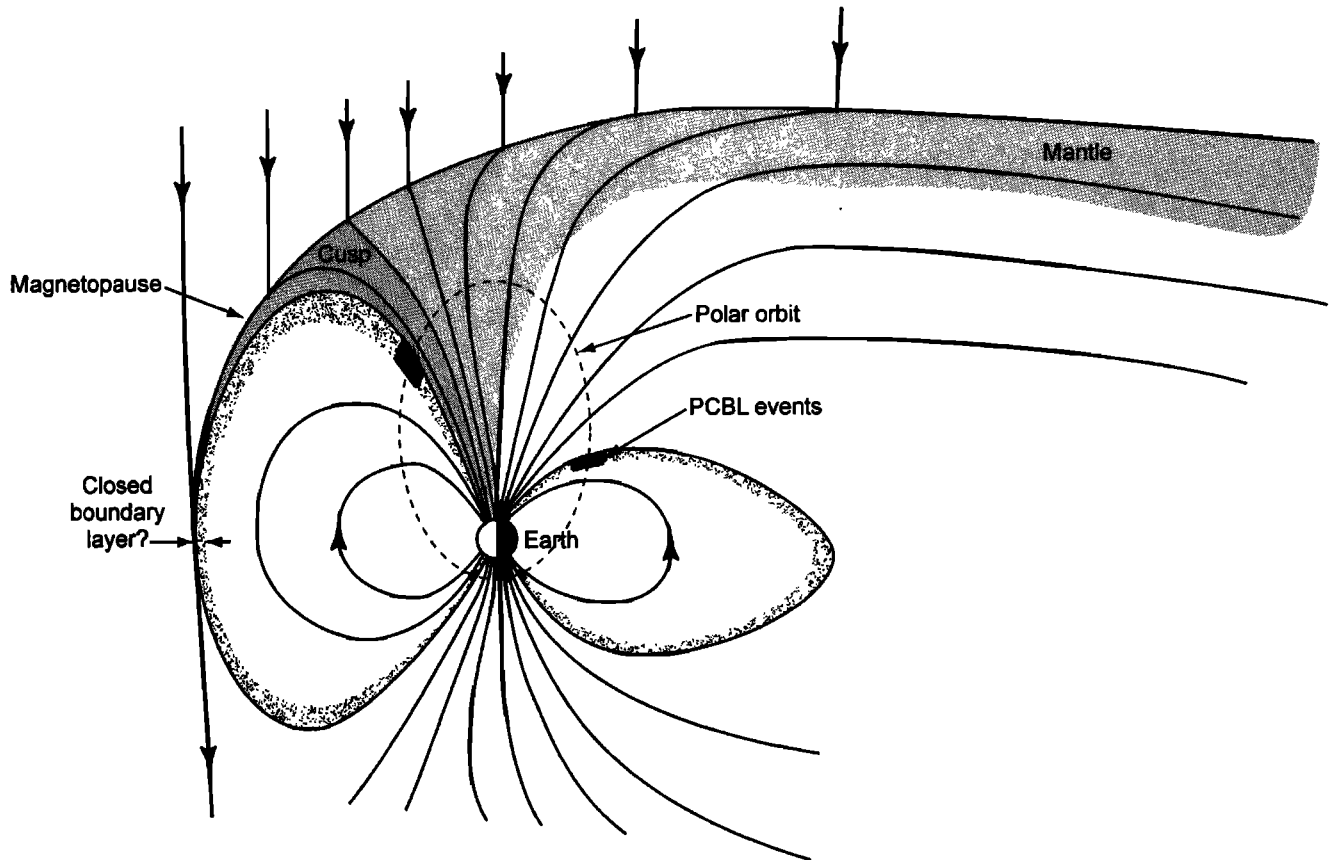
Figure 1. The Polar orbit in the magnetosphere. Solid bars indicate the four crossings of the polar cap boundary layer (PCBL) per orbit, two near apogee and two near perigee.

speeds; overlapping packets occurred quite infrequently, however), averages were calculated and stored. This method of time-tagging the solar wind data parcels to the arrival time at the magnetosphere allows additional delay times (such as due to substorms) to be considered as well. Detailed descriptions of the magnetic field and plasma instruments are given by *Lepping et al.* [1995] and *Ogilvie et al.* [1995], respectively.

3. PCBL Wave Global Survey

Figure 1 shows the orbit of the Polar spacecraft through the magnetosphere. Polar apogee occurs (during the interval of study) in the Northern Hemisphere at ~8 R_E, and the perigee occurs in the Southern Hemisphere at ~1.8 R_E. Solid bars indicate approximate locations where the "broadband" waves were detected. The locations of wave detection bound magnetic field lines that map into the polar cap, and thus they are called polar cap boundary layer waves [*Tsurutani et al.*, 1998a; *Lakhina and Tsurutani*, 1999]. The figure shows waves detected during a noon-midnight local time trajectory. The field lines that the spacecraft crosses on the dayside are believed to map into the low-latitude boundary layer, and those crossed on the nightside map into the near-Earth plasma sheet.

The PCBL waves were identified in the SFR spectrograms, independent of knowledge of spacecraft location. The criterion for a broadband wave event was intensities greater than 10^{-9} V^2 m^{-2} Hz^{-1} at ~30 Hz (the PCBL waves are generally quite broadbanded, and thus an intensity criterion set at one

particular frequency is sufficient; this analysis was done by hand. It should be noted, however, that higher-frequency narrowband waves might be missed by this survey). The start and stop times of the waves were noted and recorded. With satellite orbital information, these data were tagged as to their magnetic local time and magnetic latitude. The location of detection of the E waves is indicated in Figure 2. The location of detection in the Northern Hemisphere corresponds to the near-apogee waves, and the wave detection in the Southern Hemisphere corresponds to the near-perigee waves. Waves were detected in 96% of the crossings. The waves are essentially a permanent feature of this latitudinal region, both near apogee and near perigee.

There are several remarkable features in this display of the latitude-local time distributions. First, the longitudinal locations (both north and south) of the waves are continuous, forming "ovals" around the two magnetic poles. The second important feature to note is that the shape and location are essentially identical to the *Feldstein and Starkov* [1970] auroral oval. The waves are detected at high, ~75°, magnetic latitudes near local noon compared with the ~65° location at local midnight. This is essentially the same shape and distribution of the "Feldstein" auroral oval.

4. Interplanetary Control of Wave Intensities?

As previously mentioned, "enhanced" wave amplitudes were detected in almost every (96%) Polar pass of this region bounding the polar cap. Although the waves were almost always present, the intensity varied by many orders of magni-
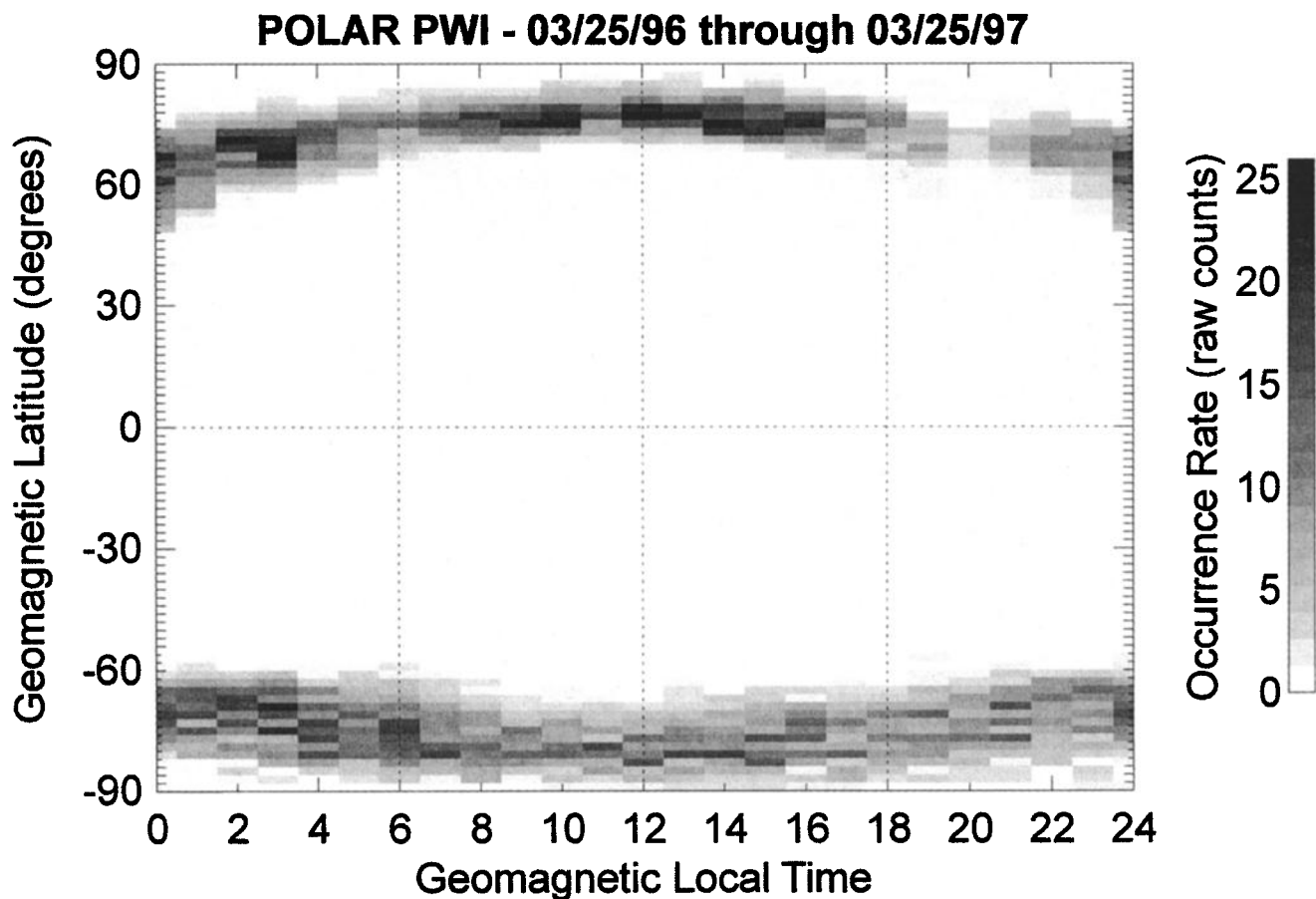
POLAR PWI - 03/25/96 through 03/25/97

Figure 2. The latitude-local time dependence of PCBL waves. On top is the distribution of the near-apogee events, and on bottom are the near-perigee events. The location of the waves is essentially the same as the auroral oval. The waves are at ~65° magnetic latitude near midnight and at ~75° near local noon.

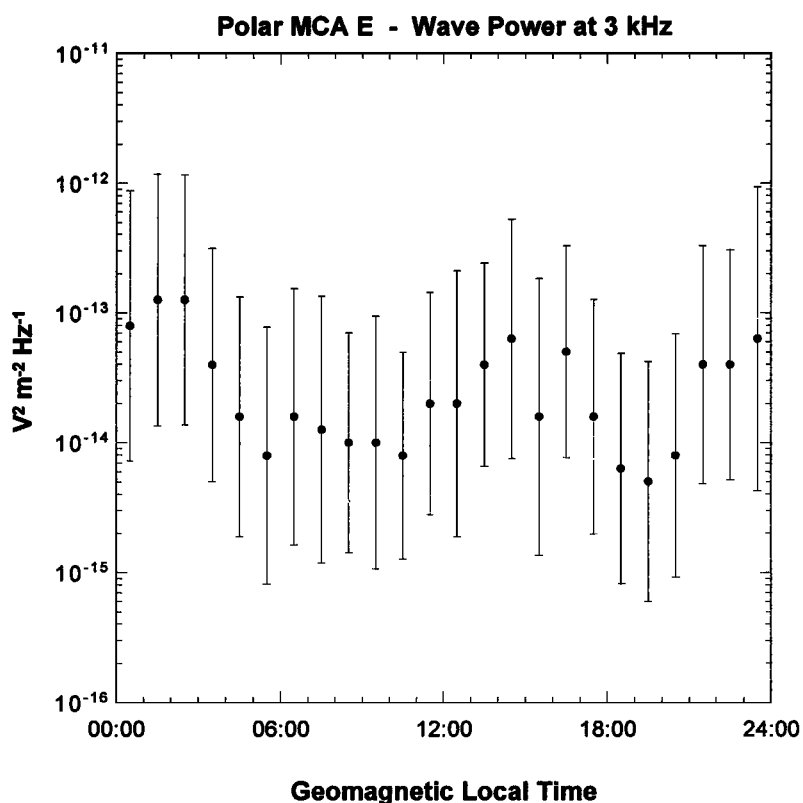**Figure 3.** The wave intensities as a function of local time. The data points are the averages of the wave 10-min log power values binned into 1-hour local time intervals. The bars are ±1 standard deviation.

tude from pass to pass and even from minute to minute (see similar discussion of LLBL wave variability by *Anderson et al.* [1982] and the many other low-latitude wave observations referenced in this paper). Figure 3 is a local time distribution of the intensity of the electric waves in the 3-kHz E spectral channel. Averages for each hour in GMLT were calculated using the MCA data. The log of the wave power average for each 10-min event was calculated, and all events were averaged. Thus, for each hour of local time, the wave log power averages and standard deviations ($\pm 1\sigma$) for all events were determined. The latter two quantities are shown in Figure 3.

Figure 3 shows that the 3-kHz E waves exhibit more than 4 orders of magnitude intensity variations, even though 10-min averages were taken. The wave intensities are the highest just past midnight (0100-0200 LT) ($\sim 10^{-13}$ V^2 m^{-2} Hz^{-1}) and just

past noon (1300-1400 LT). Local minima in average intensities exist near dawn (0500-1000 LT) and dusk (1800-2100 LT) ($\sim 5 \times 10^{-15}$ V^2 m^{-2} Hz^{-1}). The difference in average wave intensity from the maximum intensity region (0100-0200 LT) to the minimum intensity region (1800-1000 LT) is about two standard deviations. Other wave frequency channels were examined, with similar results. These are not shown for purposes of space.

The noon sector (1000-1400 LT) 562-Hz electric wave (log) intensities are shown in Figure 4 as a function of solar wind parameters. There seems to be no obvious relationship between the wave intensities and solar wind ram pressure (mNV_{SW}^2) (Figure 4d). There is a slight intensity dependence on interplanetary magnetic field (IMF) B_z (Figure 4a). The more negative B_z is, the higher is the wave intensity (statisti-
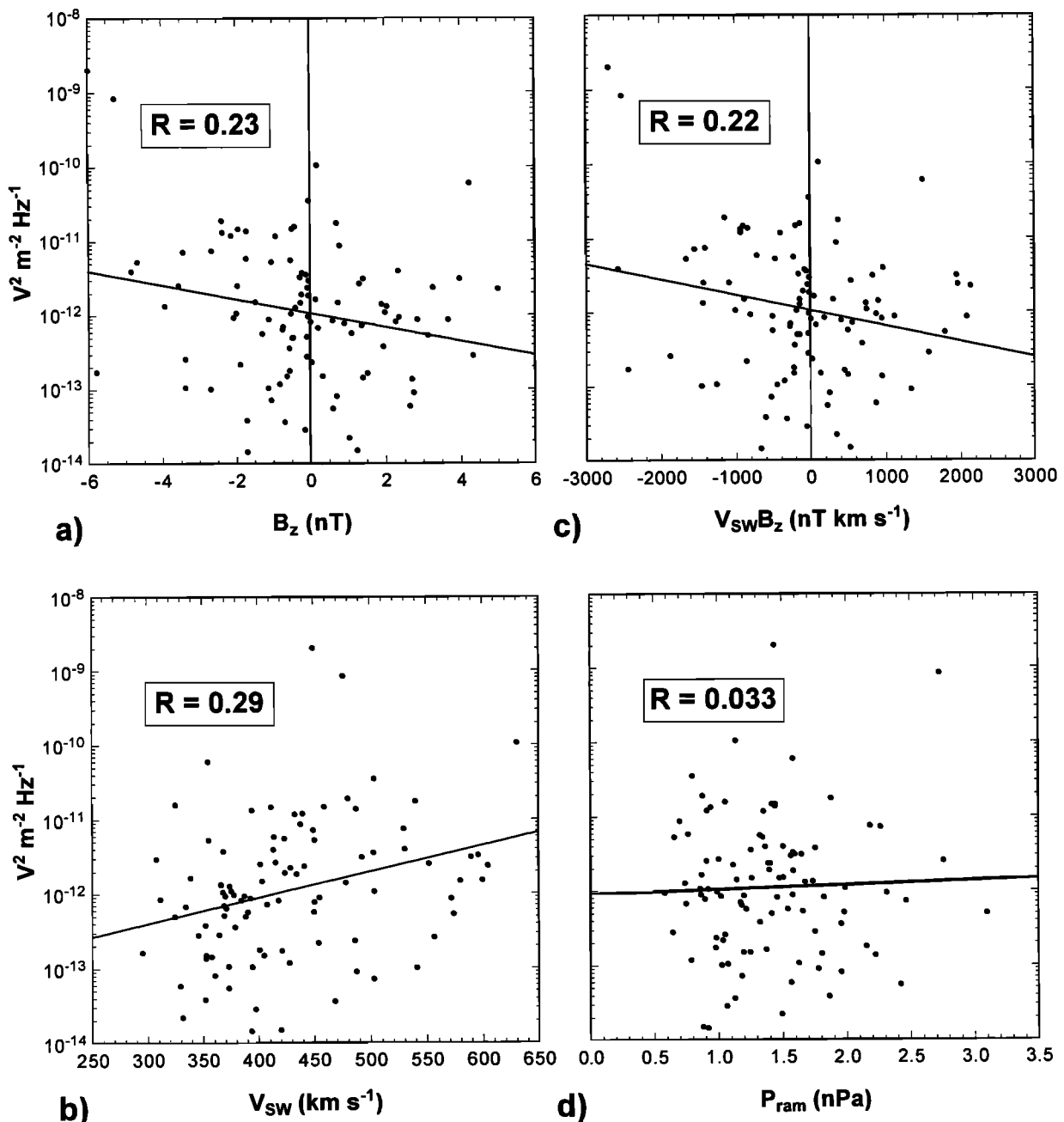

Figure 4. The wave intensity dependences on various interplanetary (Wind) parameters. The noon 562-Hz electric waves are examined here. Other wave frequencies showed similar dependences.
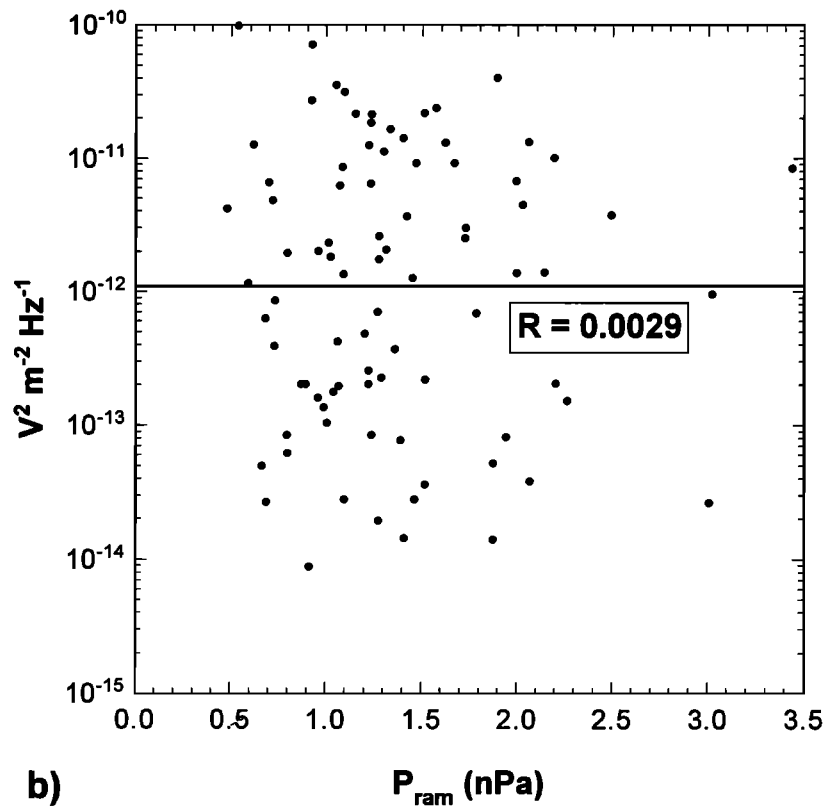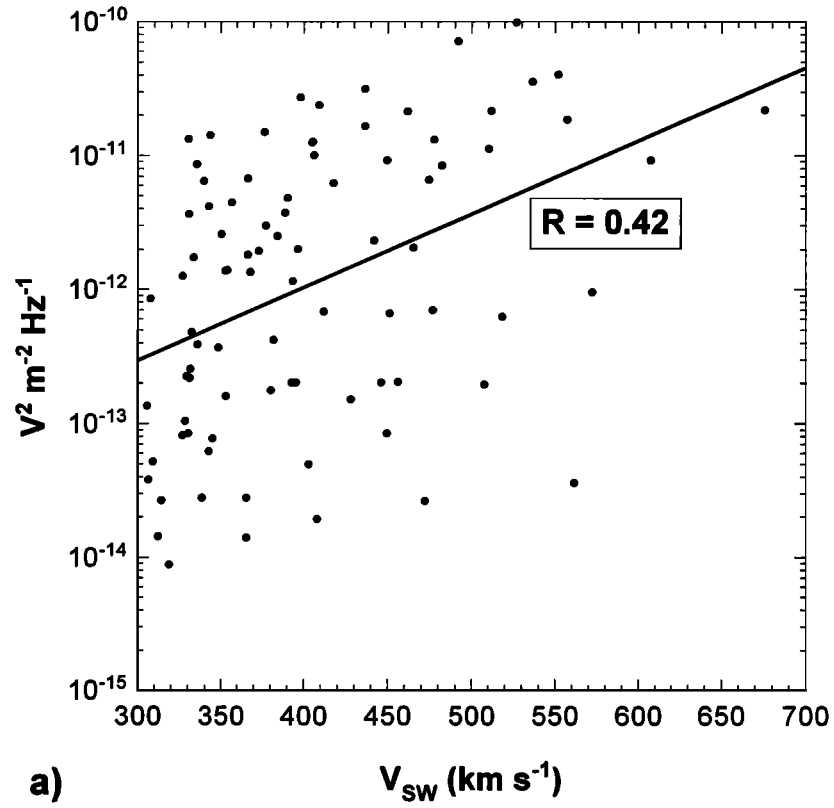
Figure 5. Same as for Figure 4, but for dusk sector (1600-2000) local times. There is a slight dependence of wave intensity on solar wind speed.

cally). The R value, associated with the regression fit, is equal to 0.23. There is a slight wave intensity dependence on V_{sw}. The R value is 0.29. There is also a slight VB_z relationship with wave intensity, as expected. Other solar wind parameters did not show any obvious relationship with wave intensity in this local time sector. Other wave frequencies were examined, with similar results. For brevity, the other figures are again not displayed.

The waves detected at dusk show a slight dependence on V_{sw}, illustrated in Figure 5a. The value R is equal to 0.42. The wave intensity increases with increasing solar wind velocity. There is little or no correlation with ram pressure (Figure 5b).

There were no AE indices available for this year of study. Thus, to determine the midnight sector wave intensity dependences, a time-lagged IMF B_z is used, with lags from 0 min up to 60 min analyzed. Only $B_z < 0$ was tested. The results are given in Figure 6. The cross-correlation analyses yielded moderate coefficients for 0-min to 40-min lag, indicating some dependence on substorm occurrence. The correlation coefficients were in the range of 0.27 to 0.32.

5. High Time Resolution Wave Survey

A complete survey of the nature of the waves is not possible at this time, due to the vast amount of information available. However, to give the reader a sense of the wave nature, we examine one pass for each of the four local time quadrants: noon, dawn, dusk, and midnight. We will summarize the general findings.

5.1. Dusk

We first present data from a dusk pass, the local time region where the waves are in a local minimum (in intensity). Plate 1 is a MCA plot of a PCBL pass on January 26, 1997. Polar is at 17.6 MLT, 4.9 R_E from the Earth, $L = 6.7$ and MLAT = 32°. The Kp value was 4 −. The most intense signals (in red) are present from 1330 to 1332 UT. The emissions are broadbanded, extending in frequency from 5.6 Hz to 10^4 Hz waves (the waves at the highest frequencies are not observed in this plate).

Simultaneous dc magnetic field measurements are displayed in Figure 7 (courtesy of C.T. Russell). The field deviations are noted from 1320 to 1332 UT (see the B_x component). These deviations correspond to the presence of intense currents [*Russell et al.*, 1997]. The strongest changes in the magnetic field components are detected from 1330 to 1331 UT.

For this event, there appears to be a one-to-one relationship between wave intensities and the magnetic field gradients (field-aligned currents). This is the typical case for all four local time intervals studied.

Figure 8 illustrates the waves present at the edge of the intense current region (~1332 UT). There are ~1.4-kHz (0.6 ms period) waves present in the perpendicular component of E. At this time the ambient magnetic field was ~370 nT. The electron cyclotron frequency was ~1.0 × 10^4 Hz, the proton cyclotron frequency was ~5.6 Hz, and the lower hybrid frequency was ~235 Hz. The plasma density was ~0.2 cm^{-3}, with a 0.2 cm^{-3} uncertainty in the absolute value (courtesy of F. S. Mozer). The electron plasma frequency was thus ~10^4 Hz.

The electric and magnetic components of the waves, both parallel and perpendicular to the ambient magnetic field, are illustrated. The electric waves have peak amplitudes of ±1 mV m^{-1}. There are components both parallel and perpendicular to B_0. The parallel component of E contains even higher-frequency components. These latter emissions correspond to short-duration wave packets occurring near the electron plasma frequency (not shown).

There are also ~150-Hz (6.5 ms period) magnetic component waves with amplitudes of ±5 × 10^{-3} nT present (next to the bottom panel). These waves are quasiperiodic.

Figure 9 shows power spectra for the three orthogonal E components of the waves of Figure 8. The wave power exists predominantly from 3 × 10^2 to 6 × 10^3 Hz. At 10^3 Hz, the transverse $E_\perp$ power is ~ 3 × 10^{-4} mV^2 m^{-2} Hz^{-1}, whereas $E_\parallel \approx$ 5 × 10^{-6} mV^2 m^{-2} Hz^{-1}, over an order of magnitude lower. These waves are thus predominantly transverse in this frequency range. At the highest frequencies the situation is reversed. At 6 × 10^3 Hz, $E_\parallel$ is ~10^{-4} mV^2 m^{-2} Hz^{-1} and $E_\perp$ ~2 × 10^{-5} $mV^2 m^{-2}$ Hz^{-1}. The latter frequency is close to the electron plasma frequency (unfortunately, there are uncertainties in this value).

5.2. Noon

At ~0825:55 UT on May 20 1996 (Figure 10), a "turn-on" of the electric waves was noted. This event occurred at approximately noon local time at a magnetic latitude of 77°. Kp was 1.0. At 0825:54.581 UT, the $E_\parallel$ signals appear out of background to reach 2 mV m^{-1} peak-to-peak amplitudes by 0825:54.584 UT (i.e., in a duration of ~3 × 10^{-3} s). There is little or no $E_\perp$ component in these signals. The frequency of the signals is highest at the beginning of the event and becomes lower with increasing time. There is no detectable magnetic component accompanying the signals.

The bipolar wave growth rate can be obtained from the data in Figure 10. The peak-to-peak amplitude at 0825:54.581 UT was ~0.25 mV m^{-1}. One millisecond later, at 0825:54.582 UT, the peak-to-peak wave amplitude was ~1.0 mV m^{-1}, or a factor of 4 increase. Assuming an exponential wave growth, these values indicate a growth rate scale time of ~0.72 ms. At the time of the wave event, the ambient magnetic field strength was ~205 nT and the local electron cyclotron frequency was ~5.7 × 10^3 Hz. Thus the wave growth rate was ~0.25f_{ce} for this event.

Figure 11 illustrates another wave "onset" on the same day, but at ~0827:08 UT. At ~0827:08.120 UT the signals started out of noise in $E_\parallel$. By 0827:08.137 UT (a duration of ~1.5 × 10^{-2} s), the waves had reached amplitudes of ±2 mV m^{-1}. The field fluctuations were primarily along the magnetic field. The wave amplitudes grew again starting at 0827:08.153 UT and reached ±9 mV m^{-1} by 0827:08.170 UT. At this time, there are clear transverse component fields ($E_\perp$) with magnitudes ~3-4 mV m^{-1}. The wave "growth" time for the first part of this event was about a factor of 5 times greater than that for the event shown in Figure 10.

Figure 12 shows examples of paired monopolar parallel pulses in the noon sector. The amplitudes were large, ~1.1 mV m^{-1} peak-to-peak values. Events are detected at ~0828:58.48 UT and at ~0828:58.49 and ~0828:58.50 UT. The event at 0828:58.475 UT appears to be a lone monopolar pulse.
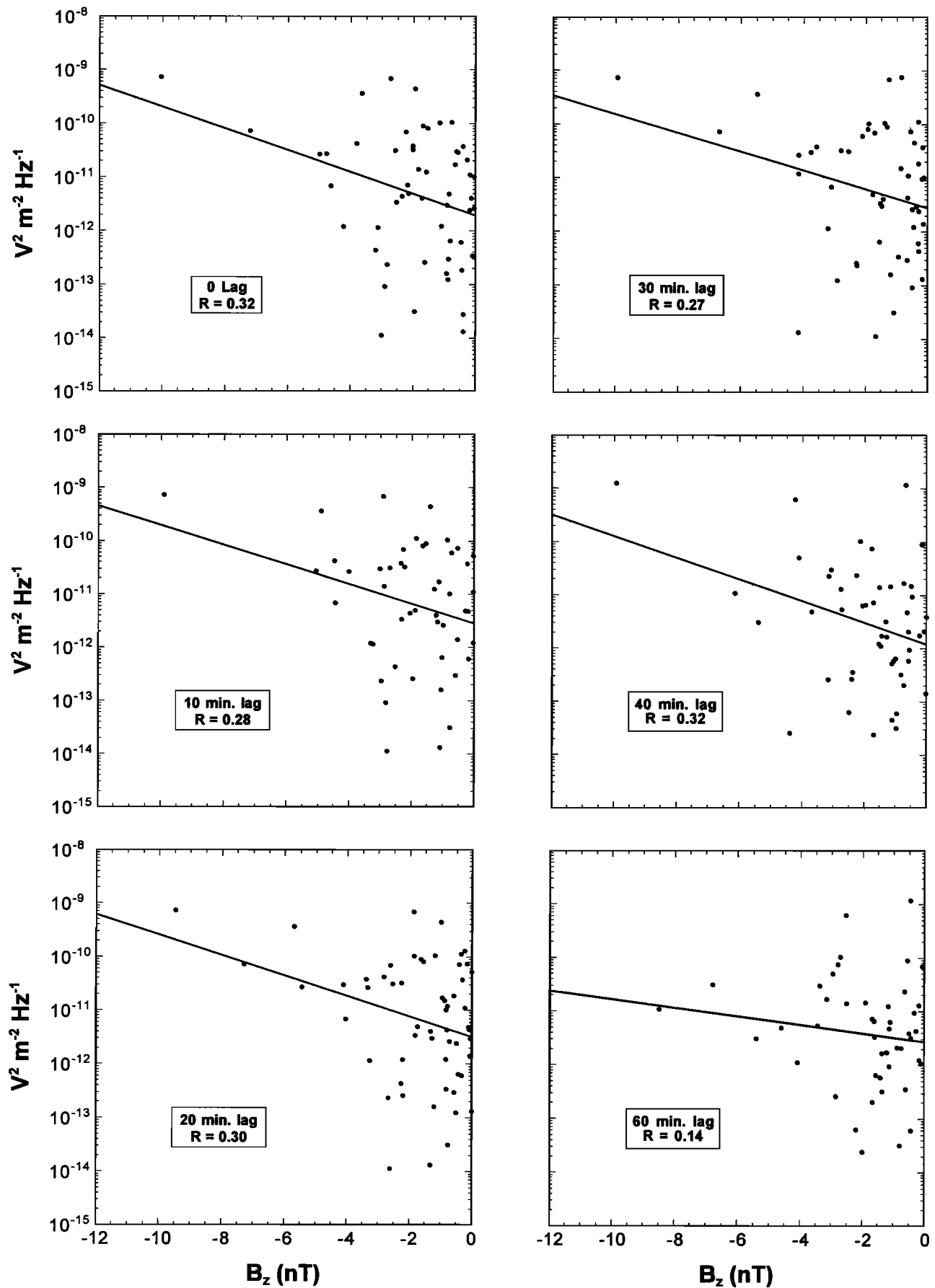
Figure 6. Local midnight (2200-0200 LT) 562-Hz electric wave intensity dependence on interplanetary B_z. Various delay times (lags) are shown.
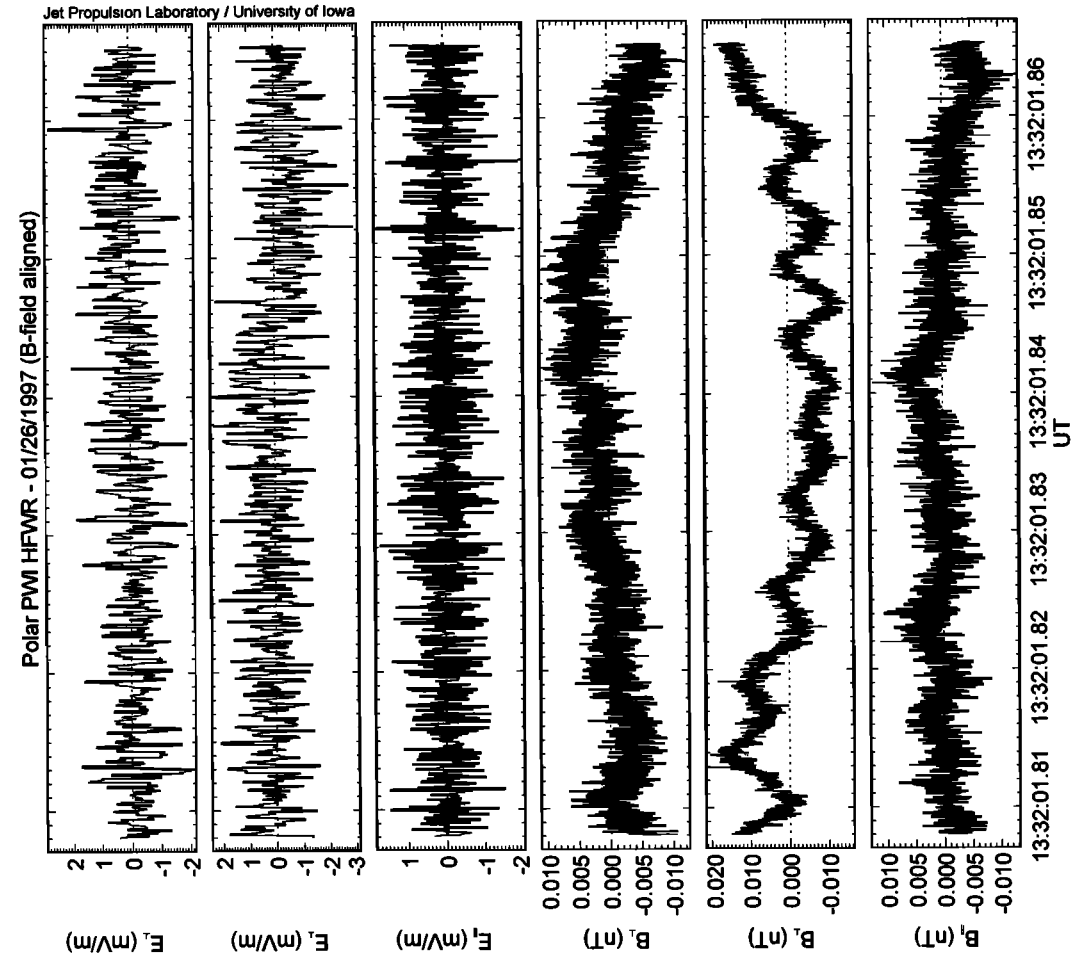
Figure 8. A ~0.05-s interval of electric and magnetic waves for the dusk event shown in Plate 1 and Figure 7. Present are ~200-Hz transverse electromagnetic waves, ~1- to 2-kHz electric waves, and ~5-kHz parallel electric waves. These waves are present near the edge of the strong current region (see Figure 7).

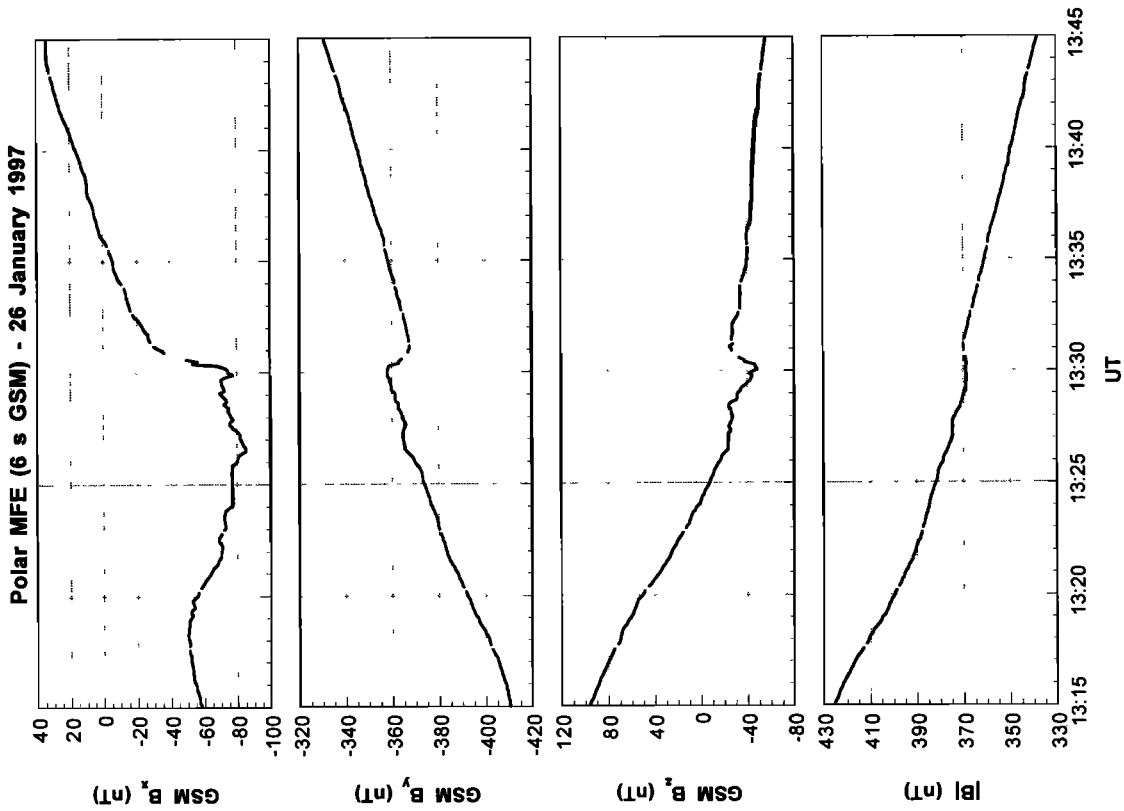**Figure 7.** The magnetic field for the event of Plate 1. The strongest field deviations (field-aligned currents) occur at ~1330-1331 UT, the same time that the PCBL waves have their greatest intensity (see Plate 1).
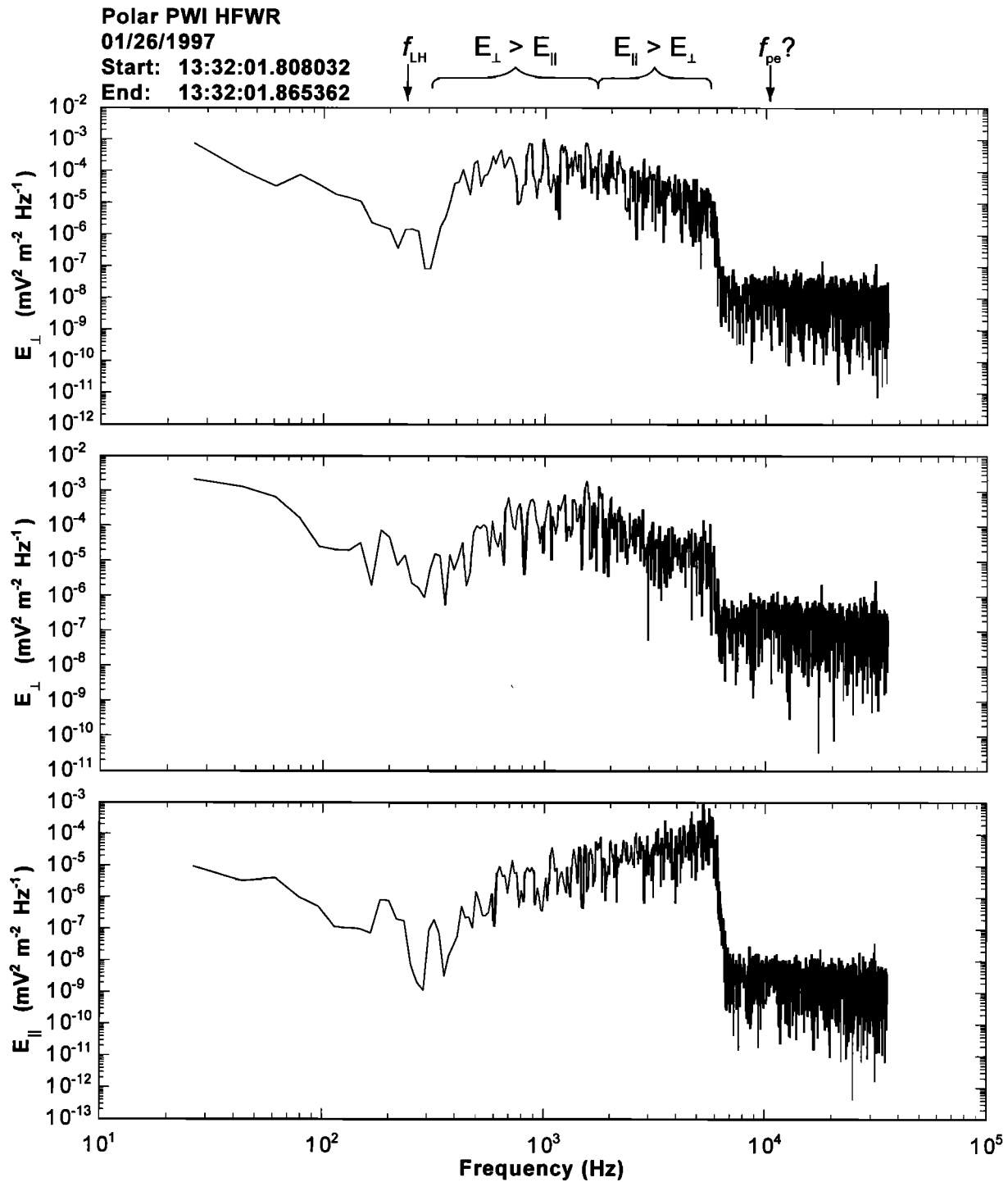
Figure 9. Power spectra for a portion of the event of Figure 8. Note that the transverse power is greater at ~1 kHz and the parallel component power dominates at ~5 kHz (when the parallel electric oscillations are present).

5.3. Dawn

Plate 2 shows the MCA plot for a dawn pass (~7.7 MLT) on December 16, 1996. From 0100 to 0300 UT, Polar went from 8.9 to 8.3 R_E and from 68° to 58° MLAT. The L value was large, >10. The Kp value was 3[+]. In this pass, the PCBL waves spanned a broad time interval (almost continuous) throughout the 2 hours. However, the most intense signals were detected from 0139 to 0148 UT and from 0200 to 0210 UT (red color).

The magnetic field for the same time interval is shown in Figure 13. There are the strong fluctuations and gradients in the GSM B_z component. Intervals of strong magnetic field gradients can be noted at 0135-0147 UT and at 0202-0210 UT. The correspondence between strong field gradients and intense waves is again readily apparent.

Figure 14a illustrates electric waves with frequencies of ~600 Hz in both $E_\perp$ and $E_\parallel$. The amplitude of $E_\perp$ is ~±0.1 mV m^{-1}, whereas $E_\parallel$ is smaller, ~±0.04 mV m^{-1}. Thus the electric oscillations are polarized primarily transverse to the ambient

Polar PWI MCA–E Eu

1997-01-26 (026) 13:15:00   SCET   1997-01-26 (026) 13:45:00

frequency (Hz)

$V^2\,m^{-2}\,Hz^{-1}$

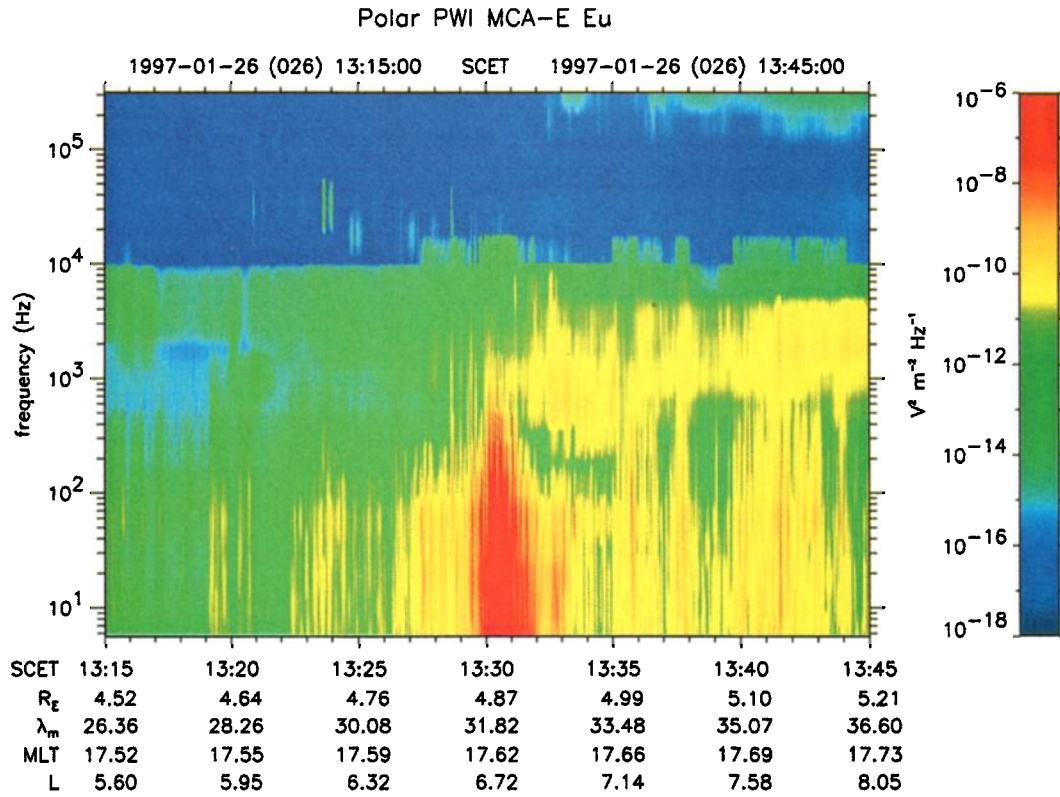| SCET	13:15	13:20	13:25	13:30	13:35	13:40	13:45
R_E	4.52	4.64	4.76	4.87	4.99	5.10	5.21
λ_m	26.36	28.26	30.08	31.82	33.48	35.07	36.60
MLT	17.52	17.55	17.59	17.62	17.66	17.69	17.73
L	5.60	5.95	6.32	6.72	7.14	7.58	8.05

Plate 1. A dusk PCBL wave event in the multichannel analyzer data format. The emissions are "broadbanded" and most intense near 1330-1331 UT.

Polar PWI MCA–E Eu

1996-12-16 (351) 01:00:00   SCET   1996-12-16 (351) 03:00:00

frequency (Hz)

$V^2\,m^{-2}\,Hz^{-1}$

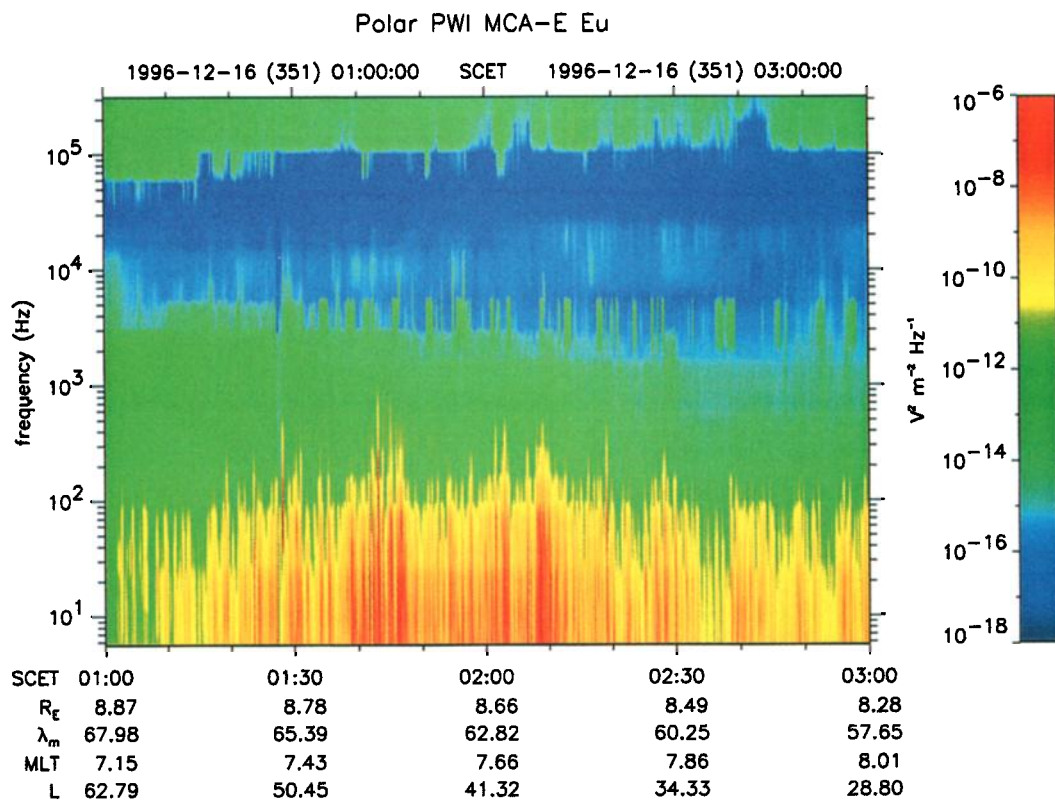| SCET	01:00	01:30	02:00	02:30	03:00
R_E	8.87	8.78	8.66	8.49	8.28
λ_m	67.98	65.39	62.82	60.25	57.65
MLT	7.15	7.43	7.66	7.86	8.01
L	62.79	50.45	41.32	34.33	28.80

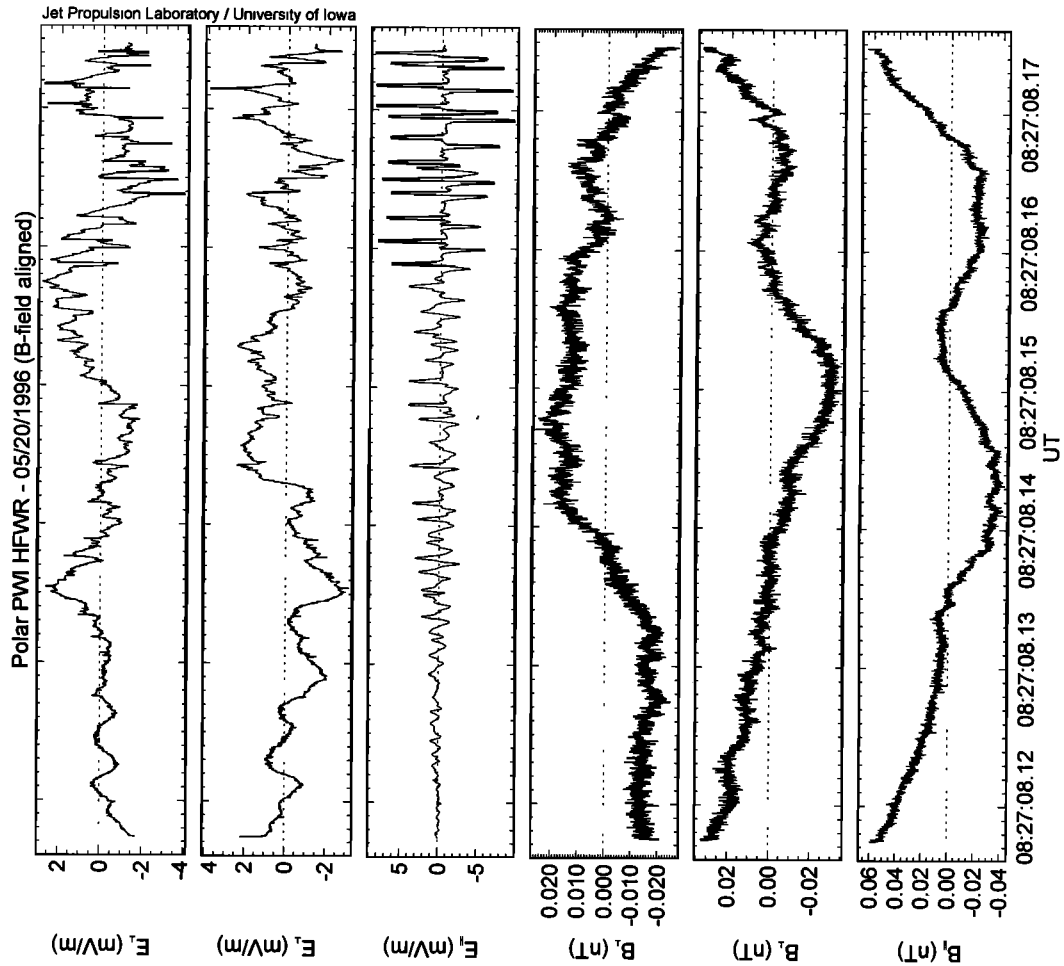**Plate 2.** A long-duration PCBL wave event detected at local dawn on December 16, 1996.

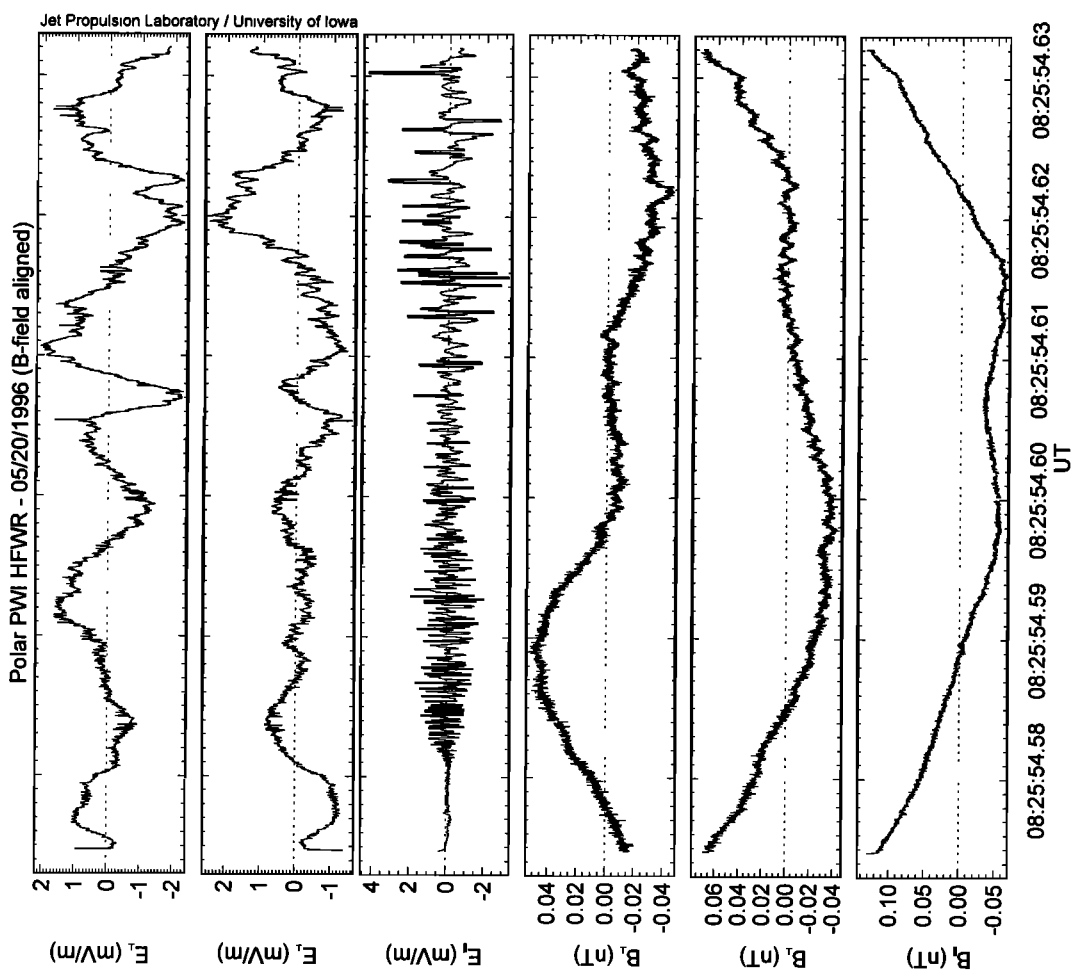**Figure 11.** Another bipolar pulse event onset. The event was detected near local noon.

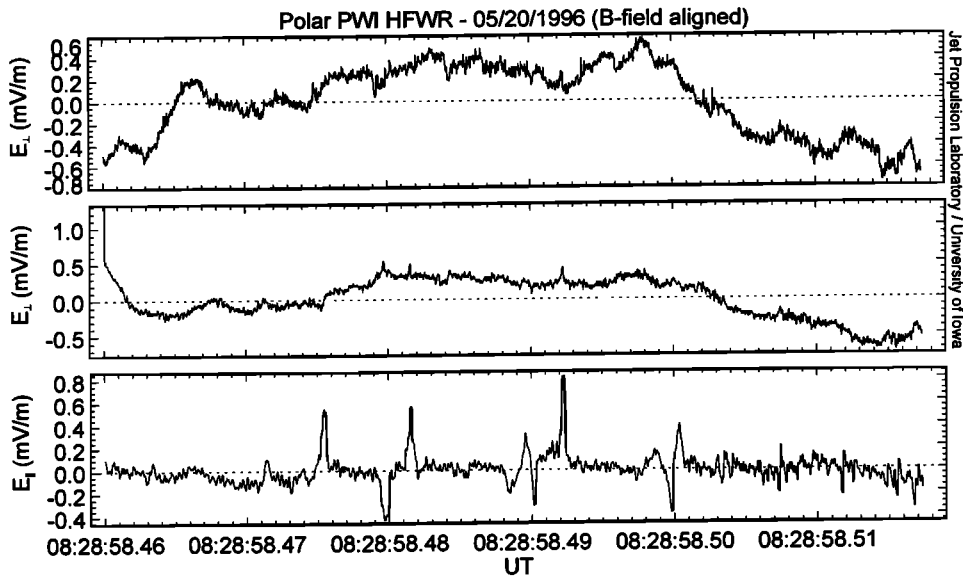**Figure 10.** The "onset" of a bipolar pulse event at local noon.

Figure 12. An example of paired monopolar parallel pulses detected in the local noon sector.
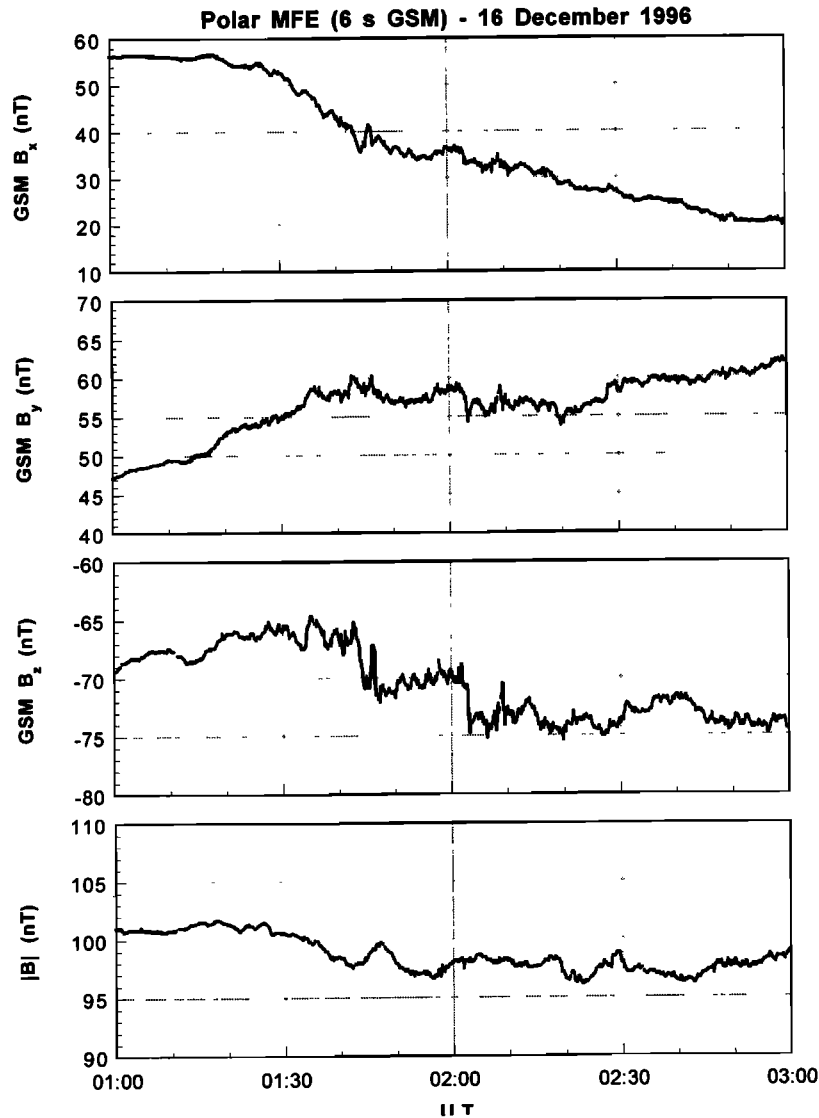
Figure 13. The magnetic field for the event of Plate 2. The strong field gradient regions and strong wave intensity regions are coincident, as in the case in Plate 1 and Figure 7.
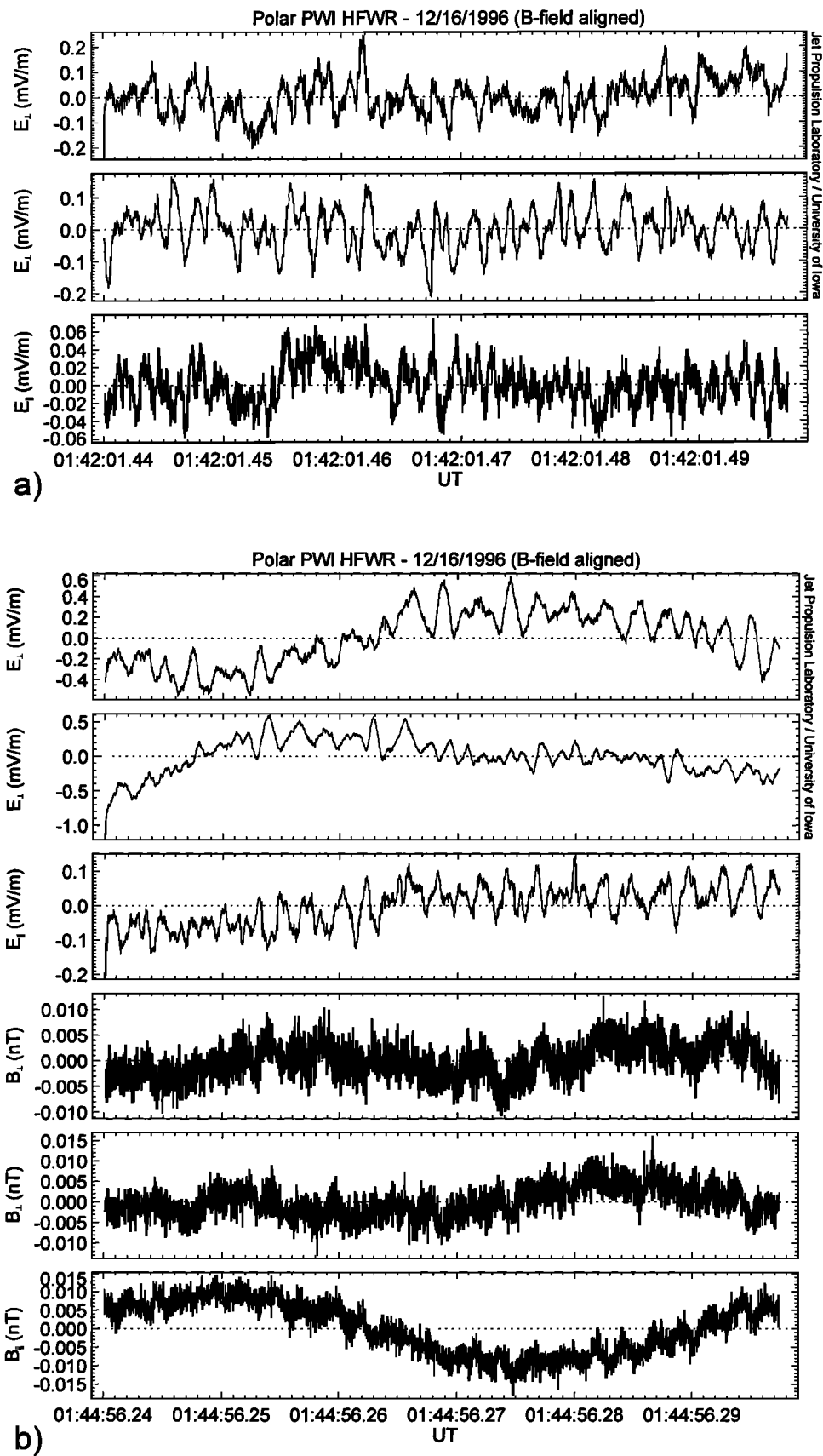
Figure 14. (a) Electric waves at ~600 Hz, polarized primarily perpendicular to B_0 There are no obvious magnetic components to the waves (not shown). (b) Waves ~3 min later in time. The frequencies of the electric waves are now lower, ~400 Hz, the wave amplitude is higher, and there is now a substantial magnetic component to the waves.

magnetic field. There was no noticeable magnetic component during this interval (not shown). There is a higher-frequency component in the $E_{\parallel}$ channel. These are parallel component electric waves at approximately the electron plasma frequency.

Figure 14b shows similar electric waves about 3 min later than in Figure 14a. The electric wave frequencies are now lower, ~400 Hz. The waves are more intense, with $E_{\perp} \approx 0.3$ mV m^{-1} peak-to-peak amplitudes and $E_{\parallel} \approx 0.1$ mV m^{-1} peak-to-peak amplitudes. In this example, there are clear magnetic components present. The amplitude is ~3 × 10^{-3} nT peak to peak in both the $B_{\parallel}$ and $B_{\perp}$ components.

5.4. Midnight

We have examined a local midnight PCBL event on April 27, 1996. Polar was at a MLT of 22.9, a distance of 5.7 R_E, a latitude of 25.3°, and an L value of 6.9. Kp was 1.0. There were two main current regions present, one near ~1010 UT and a second near 1020 UT (5.5 R_E, L=6.4). The strong PCBL wave intensities were present at only the first crossing. The wave modes present were ~3.0 × 10^{-2} nT peak-to-peak ~200-Hz electromagnetic waves, isolated bipolar pulses with peak amplitudes of ~2 mV m^{-1} and waves near the electron plasma frequency. Details of this event are not shown for brevity.

6. Summary and Discussion of Wave Modes

6.1. Electromagnetic Waves

6.1.1. The 200-Hz electromagnetic waves. Low-frequency ~200-Hz electromagnetic waves were detected in all four local time sectors. Peak amplitudes were ~±1 to 3 × 10^{-2} nT. An example of such waves detected in the dawn sector is shown in Figure 15, December 16, 1996, at 0143:33.30 UT. The wave amplitude is ~3 × 10^{-2} nT peak to peak, primarily in the $B_{\perp}$ component. The $B_{\parallel}$ component was smaller, ~1.0 × 10^{-2} nT. These ~200-Hz electromagnetic waves have frequencies similar to the "magnetic noise bursts" detected earlier by Gurnett and Frank [1977] and may indeed be the same phenomenon.

The particles responsible for the generation of this electromagnetic mode can be calculated assuming first-order cyclotron resonance. The first-order cyclotron resonance condition is

$$\omega - k_{\parallel} v_{\parallel} = \Omega^{\pm}, \tag{1}$$

where ω and $k_{\parallel}$ are the wave frequency and wave k parallel values, $v_{\parallel}$ is the particle velocity component along B_0, and $\Omega^{\pm}$ is the electron or proton cyclotron frequency. If one assumes a "normal" Doppler shift interaction between an electron beam interacting with oppositely propagating right-hand whistler-mode waves, the above expression can be written as

$$V_{\parallel} = V_{ph} (1 - \Omega^{-}/\omega). \tag{2}$$

With a measured magnetic field magnitude of ~98 nT (see Figure 13) and an electron density of ~8 × 10^{-2} cm^{-3} (F. Mozer, personal communication, 2000) the proton cyclotron frequency is ~1.5 Hz and the index of refraction ($n = f_{pe}/(f$ $f_{ce})^{1/2}$) is 12.7. It can be easily shown that the resonant parallel energy is too high for possible local wave generation by cy-

clotron interaction. Anomalous Doppler-shifted interactions with beaming protons can also be ruled out using similar arguments.

Two possibilities remain, both of which imply nonlocal generation of the electromagnetic waves. The waves could be generated in the nearby vicinity, but in regions with higher ambient plasma densities, regions where the local wave index of refraction is equal to 100. For the above parameters the resonant electrons would have to have kinetic energies of ~5 keV. Another possibility (previously mentioned by Tsurutani et al. [1998b]) is near-ionospheric generation of proton cyclotron waves [Mozer et al., 1997] by ~1-keV protons plus mode conversion to electron cyclotron (right-hand) waves. For this latter hypothesis to be viable, wave ducting is essential. Otherwise it would be difficult for the waves to propagate from the ionosphere to 6 or 7 R_E altitudes without significant attenuation.

There is a possible mechanism for local generation of the waves, but not a cyclotron resonant one. Lakhina [1980] has demonstrated that field-aligned currents and/or electron temperature anisotropies could drive the electromagnetic lower hybrid instability. Further analyses will have to be done to determine if this is the correct mechanism or not.

6.1.2. The 1- to 2-kHz electromagnetic waves. The 1- to 2-kHz electromagnetic (B) waves with amplitudes of ±5 × 10^{-3} nT were detected at dawn and noon. These waves have frequencies close to those of auroral hiss, detected at lower altitudes. Assuming first-order (normal) cyclotron resonance (electrons propagating in the opposite direction to that of the whistler-mode waves), the resonant electrons would have parallel kinetic energies of ~1.1 keV.

6.1.3. The ~5-kHz electromagnetic waves. The ~4.9-kHz waves at frequencies just below the local electron cyclotron frequency (5.5 kHz) found in a previous study [Tsurutani et al., 1998b] are reproduced here as Figure 16. The calculated resonant parallel energies are ~100 eV.

The 1- to 2-kHz electromagnetic wave generation by ~1.1-keV electron beams discussed above is most likely the same wave phenomenon, but caused by slightly different auroral electron energies. Thus variations in the auroral electron beam energies would lead to a "broad" spectrum of electromagnetic waves.

The above discussion of ~1- to 5-kHz whistler-mode wave generation by cyclotron resonant interaction with 100-eV to 1-keV electron beams was stimulated by the observations that the waves were found to be highly coherent, were often grouped in packets, and were relatively narrowbanded in frequency. The detection of these waves presented here occurred near Polar apogee, ~ 6-7 R_E from Earth, far from the auroral ionosphere. Thus, at this time, it is uncertain whether these waves are the same as "VLF hiss" detected at lower altitudes [Barrington et al., 1971; Hoffman and Laaspere, 1972; Laaspere and Johnson, 1973]. On the other hand, it should be noted that the above cited works did mention close association between hiss and auroral 100-eV to several keV electrons, so it is not only the commonality in wave mode and frequencies that makes the 1- to 5-kHz waves and hiss similarities appealing. In attempting to find a generation mechanism for auroral hiss, Maggs [1976] has argued that the generation of incoherent Cerenkov whistler radiation (by precipitating auroral electron beams) is inadequate to match the measured wave power levels. He has proposed a convective beam amplification mechanism that can produce the observed
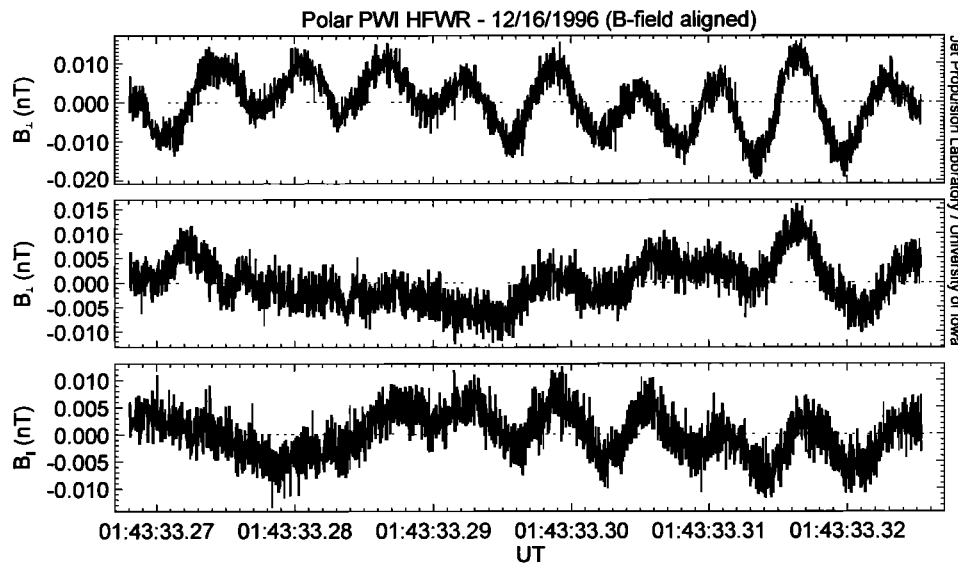
Polar PWI HFWR - 12/16/1996 (B-field aligned)

Figure 15. An example of ~200-Hz electromagnetic waves in the dawn sector. The peak-to-peak transverse amplitude is ~3 × 10^{-2} nT.

hiss bandwidth and power fluxes, when $f_{ce} < f_{pe}$. This mechanism plus that of electron cyclotron beam instabilities should be studied for the generation of the higher-altitude (presumably) lower-flux electron beam cases presented here.

6.2. Electric Waves

6.2.1. Bipolar pulses, offset bipolar pulses, and monopolar pulses. Isolated bipolar pulses and offset bipolar pulses (and monopolar pulses) were detected in all local time sectors except for dusk (however, this lack may be due to the limited sampling). In the midnight sector, the peak-to-peak amplitudes reached ~4 mV m^{-1}.

It was noted that one of the two bipolar pulse "onset" events (Figure 10) had very high "frequencies" at the beginning and lower frequencies later in the event. If all events have this profile (most do), an argument of coalescence of holes could be made. However, we did show a "contrary" event (Figure 11) that would have to be explained if one is to take the previous scenario seriously.

The onset of solitary waves near local noon shown in this paper (Figures 10 and 11) is argued to be a temporal effect. From Polar [*Mozer et al.*, 1997; *Franz et al.*, 1998] and FAST [*Ergun et al.*, 1998a, 1999] observations, the electric bipolar pulses were shown to be propagating at ~500 km s^{-1}, comparable to the electron thermal speed. Thus the hole speed is much higher than any field line convection speed or spacecraft motion. The onset of the waves with small amplitudes increasing to ~mV m^{-1} amplitudes is most easily explained as being due to local wave temporal growth.

Pottelette and Treumann [1998] have noted broadband electrostatic noise during magnetosheath plasma injection events. Timescales for both the plasma events and the waves typically last for ~1 min. We noted two clear ion injection events with correlated PCBL broadband waves in the work by *Tsurutani et al.* [1998a]. These latter events were of somewhat longer duration, 5-10 min. Preliminary examination of high time resolution data indicates that the solitary wave onsets discussed here are a subset of these broader injection events.

The bipolar electric structures observed by FAST on auroral field lines at lower altitudes [*Ergun et al.*, 1998a, 1998b] have been interpreted in terms of BGK [*Bernstein et al.*, 1957] phase space electron holes drifting along the magnetic field lines [*Muschietti et al.*, 1999a, 1999b]. *Goldman et al.* [1999a, 1999b] have explained the bipolar structures in terms of nonlinear two-stream instabilities, a mechanism similar to that proposed by *Omura et al.* [1994, 1996] and *Miyake et al.* [1998] for the electrostatic solitary waves observed by Geotail in the plasma sheet boundary layer [*Matsumoto et al.*, 1994; *Kojima et al.*, 1997].

The above mechanisms for the generation of bipolar electric structures [*Goldman et al.*, 1999a, 1999b; *Omura et al.*, 1994, 1996; *Miyake et al.*, 1998] are based on electron beams. However, there is a possibility to generate bipolar electric pulses by ion beams. *Ashour-Abdalla and Okada* [1986] have suggested ion beam generation for plasma sheet boundary layer electrostatic noise. In their simulations, electron acoustic wave generation by an ion beam would be possible if two populations of electrons (cold and hot) are present. In our case the cold electrons are present with a density of ~100 cm^{-3} (F. Mozer, personal communication, 2000). However, information about the hot electron population is not available at this time. An interesting aspect of the ion beam generation mechanism is that the instability saturates by trapping cold electrons (which eventually become hot, thus shutting off the instability). This scenario would also give rise to phase-space electron holes, as the observations from Polar and FAST suggest.

6.2.2. Lower hybrid waves. The lower-frequency "~10^3 Hz" electric oscillations show power spectral features that are similar to those shown in Figure 9. At the frequency region of peak power, ~10^3 Hz, the transverse power is substantially greater than the parallel power (~10^{-4} and ~10^{-6} mV^2 m^{-2} Hz^{-1}, respectively). However, at the high-frequency end, ~6 × 10^3 Hz, the power in E$_{\parallel}$ is slightly greater (~7 × 10^{-7} and ~3 × 10^{-7} mV^2 m^{-2} Hz^{-1}, respectively). Assuming reasonable numbers of the plasma density, temperature, and magnetic field, an estimate for the maximum magnetic component of the lower

hybrid waves [*Lemons and Gary*, 1977; *Bhatia and Lakhina*, 1980] can be made. For $E = 1$ mV m^{-1} and $\beta_e = 10^{-2}$, one gets a magnetic component of 5×10^{-3} nT, in excellent agreement with the observations (Figures 14a and 14b).

6.2.3. Upper hybrid resonance waves. Strong narrow-band electric turbulence (near the electron plasma frequency, ω_{pe}) was detected at all local times. The presence of such waves was mentioned several times before (but not shown).

These electric waves were not detected in the absence of other electric fluctuations, however.

An example of such waves is shown in Figures 17a and 17b. This is from the January 26, 1997, pass, discussed earlier. In Figure 17a, there are high-frequency waves superposed on top of lower-frequency ~10^3-Hz electric oscillations. This high-frequency component can be noted in the second $E_\perp$ channel and the $E_\parallel$ channel from ~1330:57.530 to
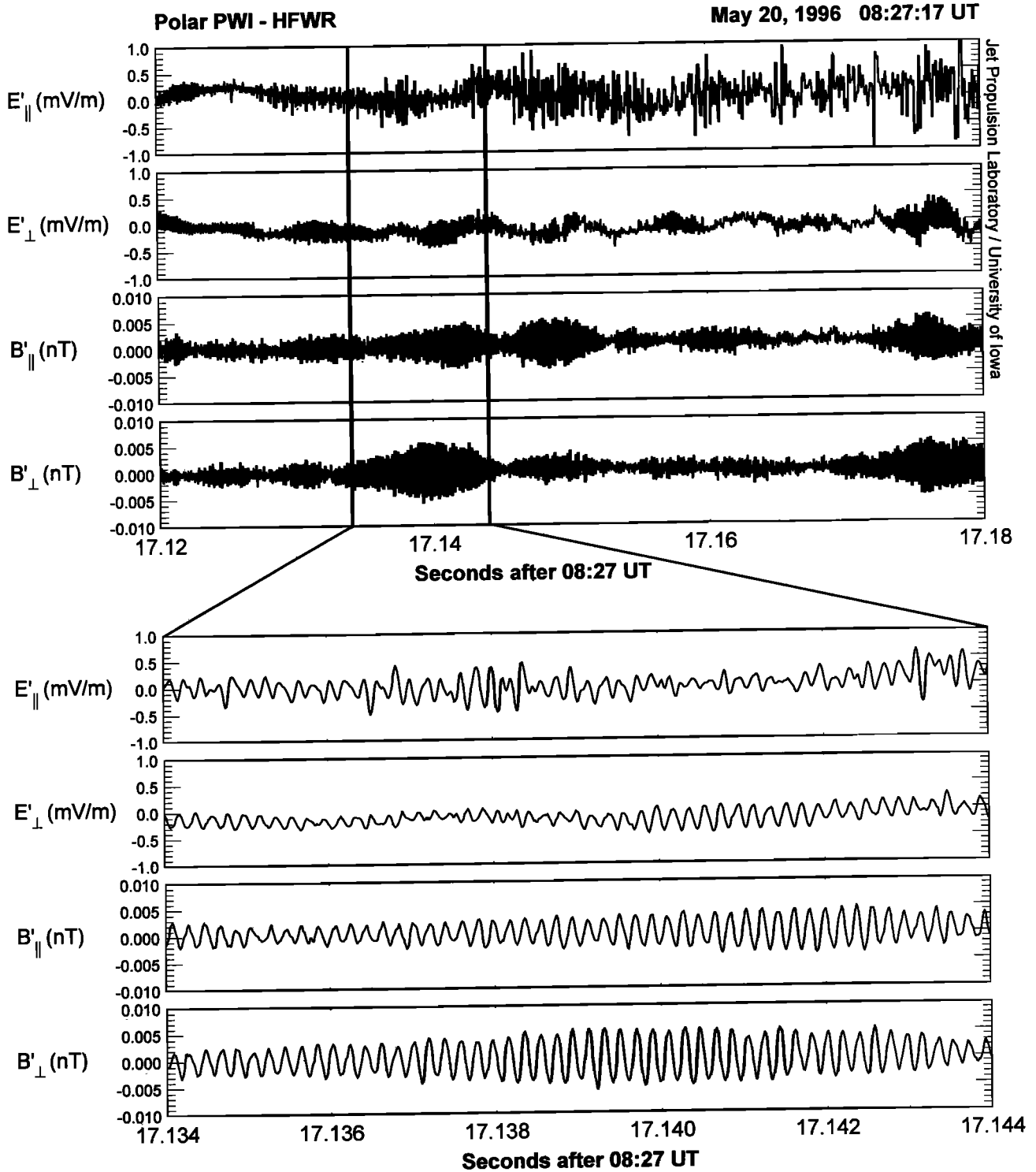

Figure 16. Electromagnetic whistler-mode waves at ~4.9 kHz. These emissions were detected near local noon. The emissions are most probably "auroral hiss" detected at lower altitudes.
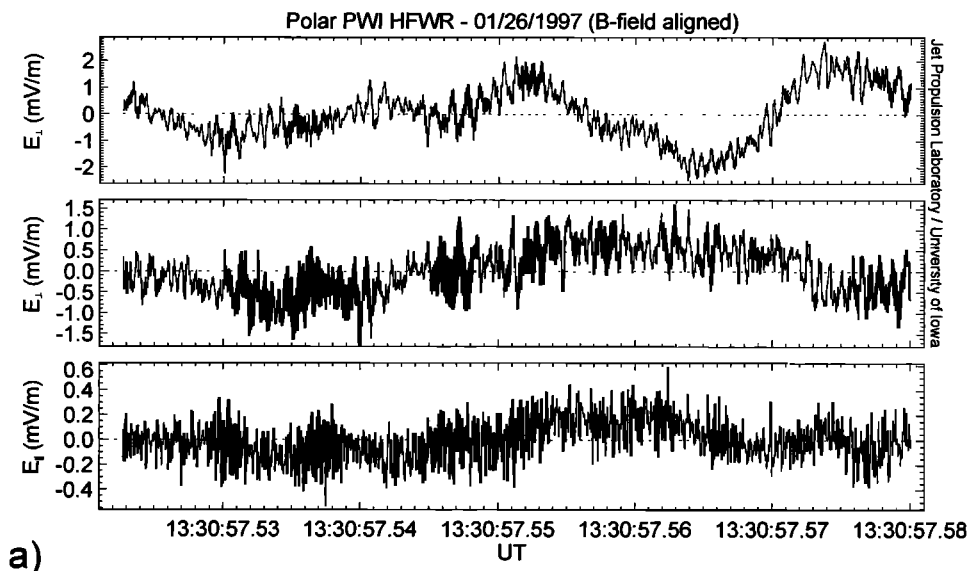
Figure 17. (a) Examples of high-frequency ~10-kHz electric waves sporadically superposed on top of ~1-kHz electric oscillations. (b) The power spectra for the same interval. The "~1 kHz waves" in actuality cover a broad frequency range from ~7 × 10^2 to ~3 × 10^3 Hz. The 10-kHz waves form a narrow peak. The dominant power of the latter waves is present in $E_\perp$.

1330:57.540 UT and from ~1330:57.544 to 1330:57.558 UT. Figure 17b illustrates the power spectra of the three components. The power is quite distinct at ~10^4 Hz. The power in the $E_\perp$ component (~1-2 × 10^{-4} mV^2 m^{-2} Hz^{-1}) is substantially greater than in the $E_\parallel$ component (~2 × 10^{-5} mV^2 m^{-2} Hz^{-1}), indicating that the wave polarization is primarily perpendicular to B. This wave mode has been identified as upper hybrid resonance noise [Gurnett and Shaw, 1973].

The electric waves are most certainly generated by low-energy electrons (see Kurth et al. [1979] for a discussion of simultaneous electron measurements). An explanation for wave growth near the electron plasma frequency has been proposed by Hubbard and Birmingham [1978]. However, the relationship between the high-frequency (~10-kHz) oscillations and the lower-frequency (~1-kHz) electric waves (Figure 17a) is yet to be established. Singh et al. [2001] have simulated a weak electron beam injection ($n_b/n_0 = 10^{-1}$, $V_b/V_{th} = 4$). At the initial stage, waves at the plasma frequency are generated. These waves progressively disappear, followed by the dominance of lower hybrid waves. This lasts from 200 < t_{fpe} < 1000. This stage is followed by another in which the high-frequency waves appear again.

This mechanism could explain the superposition of high-frequency plasma waves on top of lower hybrid waveforms. However, the observation of higher power in the $E_\perp$ component as compared with the $E_\parallel$ component suggests that high-frequency waves are probably the sideband at $f = f_{pe} + f_{lh}$ rather than the electron plasma waves. Here f_{lh} represents the lower hybrid wave frequency.

7. Summary and General Conclusions

The PCBL waves were shown to have a latitude dependence that is essentially identical to the Feldstein auroral oval. The wave amplitudes are most intense where there are strong magnetic field gradients (field-aligned currents). The nature of the electric structures is quite similar to those detected at

lower altitudes by experiments on Viking, Freja and FAST [Böstrom et al., 1988; Pottelette et al., 1990; Dubouloz et al., 1991a, 1991b; Mälkki et al., 1993; Dovner et al., 1994; Eriksson et al., 1997; Ergun et al., 1998a, 1998b, 1999]. Thus one obvious conclusion is that the PCBL waves are on auroral zone magnetic field lines. These same magnetic field lines most likely map into the LLBL region of the magnetosphere at higher altitudes.

The apogee wave intensities are somewhat lower than observed near the ionosphere (Polar perigee events). However, the decrease with altitude is not commensurate with a simple dependence on wave spreading with magnetic field line divergence. The wave decrease is much less than such a mechanism could account for [Tsurutani et al., 1998a]. The observations of bipolar pulses (nondispersed solitary waves) and offset bipolar pulses and monopolar pulses (dispersed solitary waves) at Polar near-apogee altitudes leads to the argument that Polar is detecting both freshly created waves and also evolved waves/structures; that is, there is a mixture of electric structures originating from different locations (local and nonlocal) along the field lines. The generation of the various modes of waves is most likely related to near-ionosphere particle acceleration with further particle beaming as the particles are adiabatically decompressed as they propagate to higher-altitude, lower ambient magnetic field regions. These field-aligned particles are also believed to carry a part of the field-aligned currents associated with the polar cap/magnetospheric convection processes [Carlson et al., 1998]. Thus, from this scenario, the particle beams, plasma waves, and field-aligned currents are all related to the solar wind-magnetospheric interaction. The free energy available in the field-aligned currents and gradients in the currents, plasma densities, and magnetic fields can drive several plasma instabilities that can lead to the observance of the "broadband" plasma waves [Lakhina and Tsurutani, 1999]. This local growth of waves at all altitudes should occur if this picture is a correct one.
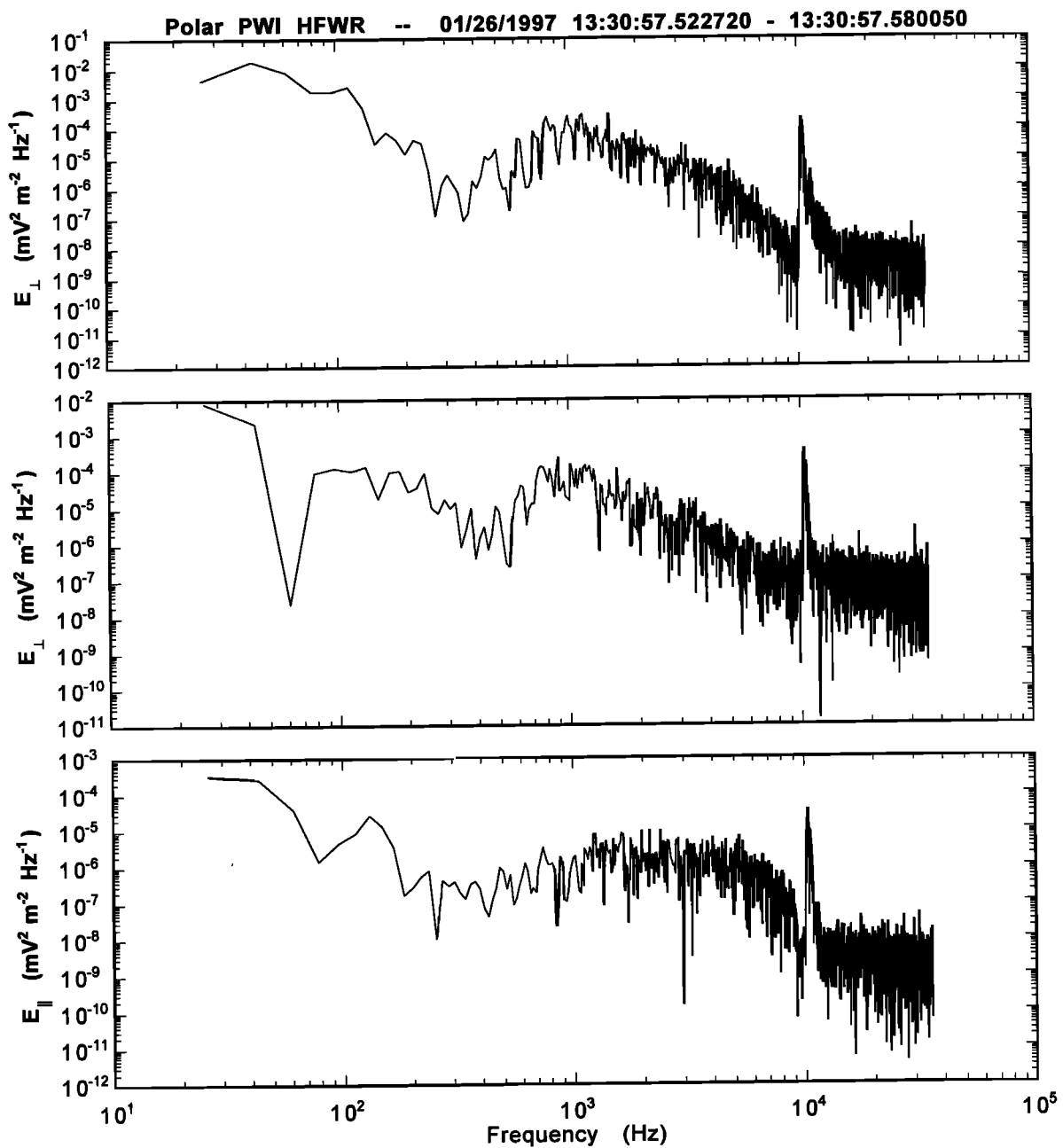
Figure 7. (continued)

The noontime waves have been shown to be more intense during intervals when the interplanetary magnetic fields were southwardly directed, or under magnetic field reconnection conditions. This has been shown for both the PCBL waves shown (here) and for LLBL waves [*Tsurutani et al.*, 1989]. Enhanced dayside magnetic reconnection will lead to greater field-aligned currents (a natural consequence) and hence greater wave amplitudes. Similar statements can be made for the near-midnight waves. Stronger nightside magnetic reconnection during substorms and storms will lead to the strongest field-aligned current system and thus the greatest wave amplitudes (as was statistically detected).

In many ways, most of the midnight and noon interplanetary field/substorm wave dependences may be not so surpris-

ing, perhaps almost expected. The most interesting regions are local dawn and dusk. Here the wave intensities are largest when the solar wind speed is the highest, indicating that a viscous-like mechanism [*Axford and Hines*, 1961; *Tsurutani and Gonzalez*, 1995] may predominate. It should also be noted that PCBL waves are found to be clearly present 96% of the time and LLBL waves are clearly present 85% of the times [*Tsurutani et al.*, 1989], independent of B_z orientation. Thus the presence of the waves and field-aligned currents could argue for a continuous, low-level viscous interaction at the flanks of the magnetopause.

The continuous presence of the PCBL/LLBL/auroral zone waves indicates that charged particles will not be confined to their field lines but will be able to diffuse into other regions

of space [*Tsurutani and Thorne*, 1982] by parasitically interacting with the waves. Cross-field diffusion of magnetosheath plasma onto closed LLBL field lines and trapped magnetospheric plasma out into the magnetosheath can be accomplished by resonant interactions with these waves. For a review of the latter process, see *Lakhina et al.* [2000].

These global auroral processes should occur at all magnetospheres where there is a strong interaction between the solar wind and the magnetosphere. Boundary layer physics at Jupiter and Saturn will be studied in the near future using Cassini data in order to determine the similarities and differences to the Earth's case.

References

Anderson, R.R., C.C. Harvey, M.M. Hoppe, B.T. Tsurutani, T.E. Eastman, and J. Etcheto, Plasma waves near the magnetopause, *J. Geophys. Res., 87*, 2087, 1982.

Ashour-Abdalla, M., and H. Okada, Electron acoustic instabilities in the geomagnetic tail, *Geophys. Res. Lett., 13*, 366, 1986.

Axford, W.I., and C.O. Hines, A unifying theory of high-latitude geophysical phenomena and geomagnetic storms, *Can. J. Phys., 39*, 1433, 1961.

Barrington, R.C., T.R. Hartz, and R.W. Harvey, Diurnal distribution of ELF, VLF, and LF noise at high latitude as observed by Alouette 2, *J. Geophys. Res., 76*, 5278, 1971.

Bhatia, K.G., and G.S. Lakhina, Drift loss cone instability in the ring current and plasma sheet, *Proc. Indian Acad. Sci., 89*, 99, 1980.

Bernstein, I.B., J.M. Greene, and M.D. Kruskal, Exact nonlinear plasma oscillations, *Phys. Rev. Lett., 108*, 546, 1957.

Böstrom, R., G. Gustafsson, B. Holback, G. Holmgren, H. Koskinen, and P. Kintner, Characteristics of solitary waves and weak double layers in magnetospheric plasma, *Phys. Rev. Lett., 61*, 82, 1988.

Bounds, S.R., R.F. Pfaff, S.F. Knowlton, F.S. Mozer, M.A. Temerin, and C.A. Kletzing, Solitary potential structures associated with ion and electron beams near 1 R_E altitude, *J. Geophys. Res., 104*, 28,709, 1999.

Carlson, C.W., R.F. Pfaff, and J.G. Watzin, The FAST auroral snapshot (FAST) mission, *Geophys. Res. Lett., 25*, 2013, 1998.

Dovner, P.O., A.I. Eriksson, R. Böstrom, and B. Holback, Freja multiprobe observations of electrostatic solitary structures, *Geophys. Res. Lett., 21*, 1827, 1994.

Dubouloz, N., R. Pottelette, M. Malingre, G. Holmgren, and P.A. Lindqvist, Detailed analysis of broadband electrostatic noise in the dayside auroral zone, *J. Geophys. Res., 96*, 3565, 1991a.

Dubouloz, N., R. Pottelette, M. Malingre, and R.A. Treumann, Generation of broadband electrostatic noise by electron acoustic solitons, *Geophys. Res. Lett., 18*, 155, 1991b.

Ergun, R.E., et. al., FAST satellite observations of large-amplitude solitary structures, *Geophys. Res. Lett., 25*, 2041, 1998a.

Ergun, R.E., C.W. Carlson, J.P. Fadden, F.S. Mozer, L. Muschietti, I. Roth, and R. Strangeway, Debye-scale plasma structures associated with magnetic-field-aligned electric fields, *Phys. Rev. Lett., 81*, 826, 1998b.

Ergun, R.E., C.W. Carlson, L. Muschietti, I. Roth, and J.P. McFadden, Properties of fast solitary structures, *Nonlinear Proc. Geophys., 6*, 187, 1999.

Eriksson, A.L., A. Mälkki, P.O. Dovner, R. Böstrom, G. Holmgren, and B. Holback, A statistical survey of auroral solitary waves and weak double layers, 2, Measurement accuracy and ambient plasma density, *J. Geophys. Res., 102*, 11,385, 1997.

Feldstein, Y.I., and G.V. Starkov, The auroral oval and the boundary of closed field lines of geomagnetic field, *Planet. Space Sci., 18*, 501, 1970.

Franz, J.R., P.M. Kintner, and J.S. Pickett, Polar observations of coherent electric field structures, *Geophys. Res. Lett., 25*, 1277, 1998.

Gendrin, R., Magnetic turbulence and diffusion processes in the magnetopause boundary layer, *Geophys. Res. Lett., 10*, 769, 1983.

Goldman, M.V., M.M. Oppenheim, and D.L. Newman, Nonlinear two-stream instabilities as an explanation for auroral bipolar wave structures, *Geophys. Res., Lett. 26*, 1821, 1999a.

Goldman, M.V., M.M. Oppenheim, and D.L. Newman, Theory of localized bipolar wave-structures and nonthermal particle distributions in the auroral ionosphere, *Nonlinear Proc. Geophys., 6*, 221, 1999b.

Gurnett, D.A., and R.R. Shaw, Electromagnetic radiation trapped in the magnetosphere above the plasma frequency, *J. Geophys. Res. 78*, 8136, 1973.

Gurnett, D.A., and L.A. Frank, A region of intense plasma wave turbulence on auroral field lines, *J. Geophys. Res., 82*, 1031, 1977.

Gurnett, D.A., R.R. Anderson, B.T. Tsurutani, E.J. Smith, G. Paschmann, G. Haerendel, S.J. Bame, and C.T. Russell, Plasma wave turbulence at the magnetopause: Observations from ISEE 1 and 2, *J. Geophys. Res., 84*, 7043, 1979.

Gurnett, D.A., et al., The Polar plasma wave instrument, *Space Sci. Rev., 71*, 597, 1995.

Hoffman, R.A., and T. Laaspere, Comparison of very low frequency auroral hiss with precipitating low-energy electrons by the use of simultaneous data from two Ogo 4 experiments, *J. Geophys. Res., 77*, 640, 1972.

Hubbard, R.F., and T.J. Birmingham, Electrostatic emissions between electron gyroharmonics in the outer magnetosphere, *J. Geophys. Res., 33*, 4837, 1978.

Kojima, H., H. Matsumoto, S. Chikuba, S. Horiyama, M. Ashour-Abdalla, and R.R. Anderson, Geotail waveform observations of broadband/narrowband electrostatic noise in the distant tail, *J. Geophys. Res., 102*, 14,439, 1997.

Koskinen, H.E.J., R. Lundin, and B. Holback, On the plasma environment of solitary waves and weak double layers, *J. Geophys. Res., 95*, 5921, 1990.

Kurth, W.S., J.D. Craven, L.A. Frank, and D.A. Gurnett, Intense electrostatic waves near the Upper Hybrid Resonance frequency, *J. Geophys. Res., 84*, 4145, 1979.

Laaspere, T., and W.C. Johnson, Additional results from an Ogo experiment concerning ionospheric electric and electromagnetic fields in the range 20 Hz to 540 kHz, *J. Geophys. Res., 78*, 2926, 1973.

La Belle, J., and R.A. Treumann, Plasma waves at the dayside magnetopause, *Space. Sci. Rev., 47*, 175, 1988.

Lakhina, G.S., Generation of low-frequency magnetic noise on auroral field lines, *J. Geophys. Res., 85*, 3325, 1980.

Lakhina, G.S., and B.T. Tsurutani, Broadband plasma waves in the magnetopause and polar cap boundary layers, *Surv. Geophys., 20*, 377, 1999.

Lakhina, G.S., B.T. Tsurutani, H. Kojima, and H. Matsumoto, "Broadband" plasma waves in the boundary layers, *J. Geophys. Res., 105*, 27,791, 2000.

Lemons, D.S., and S.P. Gary, Electromagnetic effects on the modified two-stream instability, *J. Geophys. Res., 82*, 2337, 1977.

Lepping, R.P., et al., The Wind magnetic field investigation, in *The Global Geospace Mission*, edited by C.T. Russell, p. 207, Kluwer Acad., Norwell, Mass., 1995.

Maggs, J.E., Coherent generation of VLF hiss, *J. Geophys. Res., 81*, 1707, 1976.

Mälkki, A., A. Eriksson, P. Dovner, R. Böstrom, B. Holback, G. Holmgren, and H.E.J. Koskinen, A statistical survey of auroral solitary waves and weak double layers, 1, Occurrence and net voltage, *J. Geophys. Res., 98*, 521, 1993.

Matsumoto, H., H. Kojima, T. Miyatake, Y. Omura, M. Okada, and M. Tsutsui, Electrostatic solitary waves (ESW) in the magnetotail-BEN waveforms observed by Geotail, *Geophys. Res. Lett., 21*, 2915, 1994.

McFadden, J.P., C.W. Carlson, and R.E. Ergun, Microstructure of the auroral acceleration region as observed by FAST, *J. Geophys. Res., 104*, 14,453, 1999.

Miyake, T., Y. Omura, H. Matsumoto, and H. Kojima, Two-

dimensional computer simulations of electrostatic solitary waves observed by Geotail spacecraft, *J. Geophys. Res., 103,* 11,841, 1998.

Mozer, F.S., R. Ergun, and M. Temerin, New features of time domain electric structures in the auroral acceleration regions, *Phys. Rev. Lett., 79,* 1281, 1997.

Muschietti, L., R.E. Ergun, I. Roth, and C.W. Carlson, Phase-space electron holes along magnetic field lines, *Geophys. Res. Lett., 26,* 1093, 1999a.

Muschietti, L., I. Roth, R.E. Ergun, and C.W. Carlson, Analysis and simulation of BGK electron holes, *Nonlinear Proc. Geophys., 6,* 211, 1999b.

Ogilvie, K.W., et al., in *The Global Geospace Mission,* edited by C.T. Russell, *p.* 55, Kluwer Acad., Norwell, Mass., 1995.

Omura, Y., H. Kojima, and H. Matsumoto, Computer simulations of electrostatic solitary waves in the magnetotail: A nonlinear model of broadband electrostatic noise, *Geophys. Res. Lett., 21,* 2923, 1994.

Omura, Y., H. Matsumoto, T. Miyake, and H. Kojima, Electron beam instabilities as generation mechanism of electrostatic solitary waves in the magnetotail, *J. Geophys. Res., 101,* 2685, 1996.

Pottelette, R., and R.A. Treumann, Impulsive broadband electrostatic noise in the cleft: A signature of dayside reconnection, *J. Geophys. Res., 103,* 9299, 1998.

Pottelette, R., M. Malingre, N. Dubouloz, B. Aparicio, R. Lundin, G. Holmgren, and G. Marklund, High-frequency waves in the cusp/cleft, regions, *J. Geophys. Res., 95,* 5957, 1990.

Rezeau, L., S. Perraut, and A. Roux, Electromagnetic fluctuations in the vicinity of the magnetopause, *Geophys. Res. Lett., 13,* 1093, 1986.

Russell, C.T., X.Y. Zhou, G. Le, P.H. Reiff, J.G. Luhmann, C.A. Cattell, and H. Kawano, Field-aligned currents in the high-altitude magnetopause: Polar initial results, *Geophys. Res. Lett., 24,* 1455, 1997.

Shaw, R.R., and D.A. Gurnett, Electrostatic bands associated with the electron gyrofrequency and plasma frequency in the outer magnetosphere, *J. Geophys. Res., 80,* 4259, 1975.

Singh, N., S.M. Loo, B.E. Wells, and G.S. Lakhina, Evolution of electron beam generated waves resulting in transverse ion heating and filamentation of the plasma, *J. Geophys. Res.,* in press, 2001.

Song, P., J. Zhu, C.T. Russell, R.R. Anderson, D.A. Gurnett, K.W. Ogilvie, and R.J. Strangeway, Properties of ELF emissions in the dayside magnetopause, *J. Geophys. Res., 103,* 26,495, 1998.

Temerin, M., K. Cerny, W. Lotko, and F. S. Mozer, Observations of double layers and solitary waves in the auroral plasma, *Phys. Rev. Lett., 48,* 1175, 1982.

Tsurutani, B.T., E.J. Smith, R.M. Thorne, R.R. Anderson, D.A. Gurnett, G.K. Parks, C.S. Lin, and C.T. Russell, Wave-particle interaction at the magnetopause: Contributions to the dayside aurora, *Geophys. Res. Lett., 8,* 183, 1981.

Tsurutani, B.T., A.L. Brinca, E.J. Smith, R.T. Okida, R.R. Anderson, and T.E. Eastman, A statistical study of ELF-VLF plasma waves at the magnetopause, *J. Geophys. Res., 94,* 1270, 1989.

Tsurutani, B.T., and R.M. Thorne, Diffusion processes in the magnetopause boundary layer, *Geophys. Res. Lett., 9,* 1247, 1982.

Tsurutani, B.T., D.J. Southwood, E.J. Smith, and A. Balogh, A survey of low frequency waves at Jupiter: The Ulysses encounter, *J. Geophys. Res., 98,* 21,203, 1993.

Tsurutani, B.T., and W.D. Gonzalez, The efficiency of "viscous interaction" between the solar wind and the magnetosphere during intense northward IMF events, *Geophys. Res. Lett., 22,* 663, 1995.

Tsurutani, B.T., et al., Plasma wave characteristics of the Jovian magnetopause boundary layer: Relationship to the Jovian aurora, *J. Geophys. Res., 102,* 4751, 1997.

Tsurutani, B.T., G.S. Lakhina, C.M. Ho, J.K. Arballo, C. Galvan, A. Boonsiriseth, J.S. Pickett, D.A. Gurnett, W.K. Peterson, and R.M. Thorne, Broadband plasma waves observed in the polar cap boundary layer: Polar, *J. Geophys. Res., 103,* 17,351, 1998a.

Tsurutani, B.T., J.K. Arballo, G.S. Lakhina, C.M. Ho, B. Buti, J.S. Pickett, and D.A. Gurnett, Plasma waves in the dayside polar cap boundary layer: Bipolar and monopolar electric pulses and whistler mode waves, *Geophys. Res. Lett., 25,* 417, 1998b.

Zhu, Z., P. Song, C.T. Russell, R.R. Anderson, D.A. Gurnett, K.W. Ogilvie, and R.J. Fitzenreiter, The relationship between ELF-VLF waves and magnetic shear at the dayside magnetopause, *Geophys. Res. Lett., 23,* 773, 1996.

J. K. Arballo, C. Galvan, B. T. Tsurutani, L. D. Zhang, and X.-Y. Zhou, Jet Propulsion Laboratory, California Institute of Technology, Pasadena, CA 91109. (Bruce.Tsurutani@jpl.nasa.gov)

D. A. Gurnett and J. S. Pickett, Department of Physics and Astronomy, University of Iowa, Iowa City, IA 52242.

T. Hada, Earth System Science and Technology, Kyushu University, Fukuoka 816-8580, Japan.

G. S. Lakhina, Indian Institute of Geomagnetism, Mumbai/Bombay 400 005, India.